Targeting Heterochromatin Eliminates Chronic Myelomonocytic Leukemia Malignant Stem Cells Through Reactivation of Retroelements and Innate Immune pathways

Donia Hidaoui[1,2,3,], Audrey Porquet[1,2,3], Rabie Chelbi[1,2,3,4], Mathieu Bohm[1,2,3,4], , Aikaterini Polyzou[5], Vincent Alcazer[6], Stéphane Depil[6], Aygun Imanci[1,2,3,4], Margot Morabito[1,2,3,], Aline Renneville[1,2,3,7], Dorothée Sélimoglu-Buet[1,2,3], Sylvain Thépot[8], Raphael Itzykson[9], Lucie Laplane[1,2,3,10], Nathalie Droin[1,2,3,7], Eirini Trompouki[5], Emilie Elvira-Matelot[1,2,3], Eric Solary[1,2,3,11] and Françoise Porteu[1,2,3,*]

1. *Inserm UMR1287, Gustave Roussy Cancer Center, 94805, Villejuif, France*.
2. *Université Paris-Saclay,*
3. *Equipe labellisée Ligue Nationale Contre le Cancer*
4. *Inovarion, 75005 Paris, France.*
5. *Institute for Research on Cancer and Aging of Nice (IRCAN), Université Côte d'Azur, INSERM, CNRS, Nice, France*.
6. *Cancer Research Center of Lyon, UMR INSERM U1052 CNRS 5286, Centre Léon Bérard, Lyon, France*
7. *INSERM US23, CNRS UMS 3655, Gustave Roussy Cancer Center, Villejuif, France.*
8. *Clinical Hematology Department, University Hospital, Angers, France.*
9. *Hematology Department, Saint-Louis Hospital, Paris, France.*
10. *Institut d'Histoire et Philosophie des Sciences et des Techniques, Université Paris I Panthéon-Sorbonne, Paris, France.*
11. *Clinical Hematology Department, Gustave Roussy Cancer Center, Villejuif, France.*

** to whom correspondence should be sent*

Françoise Porteu (francoise.porteu@gustaveroussy.fr)

INSERM U1287

Cancer Campus Gustave Roussy, PR1

114 rue Édouard-Vaillant

94805 Villejuif Cedex-France

Tel: (33) 1 42 11 23 48

Running title: Eradication of CMML HSPCs through retroelements expression.

The authors declare no potential conflicts of interest

Abstract

Chronic myelomonocytic leukemia (CMML) is a severe myeloid malignancy affecting the elderly, for which therapeutic options are limited. DNA hypomethylating agents (HMAs) provide transient responses, failing to eradicate the malignant clone. Hematopoietic stem cell (HSC) aging involves heterochromatin reorganization, evidenced by alterations in histone marks H3K9me2 and H3K9me3. These repressive marks together with DNA methylation are essential for suppressing transposable elements (TEs). In solid cancers, the antitumor efficacy of HMAs involves the derepression of TEs, mimicking a state of viral infection. In this study, we demonstrate a significant disorganization of heterochromatin in CMML HSCs and progenitors (HSPCs) characterized by an increase in the repressive mark H3K9me2, mainly at the level of TEs, and a repression of immune and age-associated transcripts. Combining HMAs with G9A/GLP H3K9me2 methyltransferase inhibitors reactivates these pathways, selectively targeting mutated cells while preserving wild-type HSCs, thus offering new therapeutic avenues for this severe myeloid malignancy.

Introduction

Chronic myelomonocytic leukemia (CMML) is a myeloid neoplasm originating from a hematopoietic stem cell (HSC). This disease usually emerges in the elderly (median age at diagnosis is 72 years) and combines dysplastic and proliferative features, therefore is classified as a myelodysplastic/myeloproliferative neoplasm[1]. Somatic mutations detected in CMML cells typically and diversely affect genes encoding epigenetic, splicing and signaling molecules. These mutations accumulate almost linearly in the stem cell compartment, with an early dominance of the clone that invades most of this compartment and a growth advantage to the most mutated cells with differentiation[2]. Such a relatively simple genotype contrasts with the heterogeneous phenotype of the disease. Consistently, abnormal DNA methylation profiles were identified as an additional feature of the disease[3-5].

CMML is a severe neoplasm with a median survival lower than 3 years in most series. The sole curative therapeutic option is allogeneic stem cell transplantation, which is difficult to implement due to age and comorbidities. Cytoreductive drugs and DNA hypomethylating agents (HMAs) are used in patients with predominantly proliferative and dysplastic CMML variants, respectivey[6]. The therapeutic response to these drugs is always transient. The response to HMAs correlates with demethylation of leukemic cell DNA with a restored hematopoiesis that contrasts with the lack of decrease in the fraction of mutated cells[4]. Thus, HMA-induced correction of hematopoietic imbalance is likely attributable to epigenetic rather than cytotoxic effects.

In accordance with the age at diagnosis, two clock-like molecular signatures were identified in CMML cells[4]. Cellular aging also involves heterochromatin reorganization[7,8], with alterations in DNA methylation and histone H3K9me2 and H3K9me3 mark patterns. Reduced H3K9me3

24 in HSCs is observed in aging or premature aging models, correlating with characteristic
25 hematopoietic changes related to aging[9-11]. DNA methylation and repressive histone marks
26 are crucial regulators of genome stability by repressing transposable elements (TEs), including
27 DNA transposons and retrotransposable elements (RTEs). RTEs, which are classified into long
28 terminal repeat (LTR) that characterize endogenous retroviruses (ERVs), and non-LTR
29 elements such as long or short interspersed elements (LINE-1/L1; SINE), utilize a copy/paste
30 mechanism to spread in the genome, causing double-strand breaks, and contribute to gene
31 regulatory networks with a potential oncogenic role[12]. TEs also serve as a source of
32 endogenous double-stranded (ds) RNA or cytoplasmic cDNA that are sensed as genomic
33 parasites, ultimately triggering a type I interferon (IFN-I) response[13]. In HSCs, TE
34 overexpression induced by irradiation and chemotherapy leads to DNA damage accumulation,
35 and creates an intrinsic sterile inflammatory context potentially contributing to functional
36 changes that generate an aging phenotype[14,15].

37 HMA activity in solid tumors was ascribed to their capacity to derepress TEs that generate a
38 type I interferon (IFN-I) and NFκB response and promote the expression tumor-associated
39 antigens[16,17]. The role of these pathways in hematological malignancies treated with HMAs is
40 less known. In the present study, we show a significant chromatin disorganization in HSPCs of
41 CMML patients compared to aged healthy donors, which repress TE expression and
42 inflammatory signaling. We also provide evidence that a combination of HMAs and H3K9me2
43 methyltranferase inhibitors could reactivate these pathways, specifically targeting the
44 mutated clone while preserving unmutated HSCs.

45

46

Results

CMML HSPCs show a decrease in inflammatory response pathways

To explore the characteristics of pathological aged hematopoiesis in CMML patients versus healthy aging, we assembled a cohort of untreated CMML patients, at the time of diagnosis, and age-matched healthy donors (herein referred to as controls) (Supplementary Table 1). Bulk RNA-sequencing (RNA-seq) analysis was performed on $CD34^+$ hematopoietic stem and progenitor cells (HSPCs) isolated from the bone marrow (BM) of 19 patients (mean age 70.6, range 49-84) and 12 age-matched healthy donors (mean age 68, range 54-91). Principal component analysis (PCA) showed separation of control and patient transcriptomes (Fig. 1a). Of 2,664 differentially expressed genes (DEGs) (adjusted pvalue <0.1), 54% were upregulated (Fig. 1b; supplementary Data 1). Gene set enrichment analysis (GSEA) examining HALLMARK and KEGG gene sets indicated that control cell transcriptomes were significantly enriched in various inflammatory, innate immune response, cytokine signaling, as well as cell cycle, P53, and apoptosis pathways (Fig. 1c; Supplementary Fig. 1a and Data 2). Gene Ontology process analysis unveiled that, beyond immune response, terms associated with chromatin remodeling and DNA packaging were enriched in controls (Fig. 1d; Supplementary Fig. 1b and Data 2). In contrast, patient cells exhibited enrichment in only a few terms related to ribosomes, vascular system development, actin, and adhesion (Fig. 1d; Supplementary Fig. 1a).

Increased expression of inflammatory genes, P53 signaling and chromatin deregulation are indicative of senescence and aging[8,18-22].The transcriptome of patient HSPCs therefore suggests a younger state compared to control HSPCs. Supporting this possibility, senescence and aging signatures were more pronounced in control cells (Fig. 1e and f; Supplementary Fig.

71 1c). Furthermore, a signature composed of genes upregulated in aged versus young human
72 BM HSCs[22] was depleted in patient cells, while genes downregulated with age were marginally
73 enriched (Fig. 1g).

74 **Chromatin is remodeled in CMML HSPCs**
75
76 We have previously shown that murine and human HSC aging is associated with a loss of
77 H3K9me3 heterochromatin mark[9,11]. Decreased expression of the heterochromatin mark
78 H3K9me2, assessed by immunofluorescence, was also detected in HSCs from aged mice and
79 in $CD34^+$ BM cells from aged individuals compared with umbilical cord blood (Supplementary
80 Fig. 2a and b). These results prompted us to analyze H3K9me3 and H3K9me2 expresssion in
81 HSPCs from patients and controls. Surprisingly, immunofluorescence analysis suggested a
82 significant decrease in H3K9me3 expression in patient cells (Fig. 2a), which was confirmed by
83 immunoblot analysis in five patients (Supplementary Fig. 2c). As H3K9me3 is a repressive
84 mark, this suggests that this epigenetic change is not responsible for the decreased expression
85 of aging and senescence genes observed in cells from CMML patients, compared to age-
86 matched control cells (Fig. 1f and g). In contrast, a significant increase in H3K9me2 expression
87 was detected by immunofluorescence in the $CD34^+$ cells of 28/29 patients (Fig. 2b), and
88 validated by immunoblot analysis in five patients (Supplementary Fig. 2d). This correlated with
89 heightened expression of the H3K9-dimethyltransferases G9A and GLP, particularly at the
90 protein level (Fig. 2c and d; Supplementary 2e and f). Increased expression of H3K9me2, G9A
91 and GLP were also observed in patient $CD34^+CD38^-CD90^+$ HSC-enriched populations
92 (Supplementary Fig. 2g-i). No correlation was found between the level of H3K9me2 in $CD34^+$
93 cells and the presence of TET2, RAS, ASXL1 or SRSF2 mutations, WBC counts, the percent of
94 BM blasts or age (Supplementary Fig2. j-m).

95 To explore the impact of these opposite modifications on two heterochromatin marks on
96 chromatin opening genome-wide, we conducted Assay for Transposase-Accessible
97 Chromatin-sequencing (ATAC-seq) experiments in $CD34^+$ cells from 4 patients and 3 controls.
98 We detected 40,335 differential peaks, with 31,110 (77%) gained and 9,245 (23%) lost in
99 CMML cells (Fig. 2e; Supplementary Data 3). Altered peaks were significantly enriched in
100 intergenic and intronic regions, while common peaks were predominantly located at the
101 transcription start sites (Supplementary Fig. 3a). Assigning differential ATAC-seq peaks to
102 genes[15] demonstrated a substantial overlap between DEGs and ATAC-seq peaks (Fig. 2f).
103 Analysis of transcription factor (TF) motifs in peaks using HOMER demonstrated specific or
104 stronger enrichment of motifs for TF involved in hematopietic differentiation (FL11, RUNX1,
105 GATA1, GATA1, NF-E2, EKLF, MAFB, MYB), TGF-β signaling (SMAD2, SMAD3, SMAD4)
106 inflammation (NFκB, IRF1, IRF3, RFX, ISRE), in ATAC-seq peaks with reduced compared with
107 gained chromatin accessibility (Fig. 2g; Supplementary Fig. 3b; Supplementary Data 4). This is
108 consistent the lower enrichment of these pathways in CMML patient cells (Fig. 1c, d;
109 Supplementary Data 2). In addition, numerous processes related to
110 immune/inflammation/NFκB signaling were associated with genes exhibiting loss of
111 chromatin accessibility (Fig. 2h; Supplementary Fig. 3c). This suggests that the attenuated
112 expression of certain immune/inflammatory response genes in patient cells might be related
113 to an altered chromatin accessibility.
114 Together, these results highlight a profound chromatin remodeling that may contribute to
115 repressing inflammatory genes in CMML compared to healthy $CD34^+$ cells.

116

117

118 **H3K9me2 is enriched at TEs in CMML HSPCs**

119 H3K9me2 is recognized as a suppressor of innate immune genes, notably exerting direct
120 control over the expression of *IFNB1* gene, encoding IFN-β, and certain IFN-stimulated genes
121 (ISGs)[23,24]. This suggests that increased H3K9me2 in CMML cells could contribute to the
122 observed decreased chromatin accessibility at immune/inflammatory genes and in their
123 expression. We therefore focused on this mark, performing H3K9me2 CUT&Tag analysis in
124 $CD34^+$ cells, comparing 4 patients with 3 controls. As expected from immunofluorescence and
125 western blot experiments, patient cells exhibited a greater number of recovered peaks
126 (15,406 ± 1,484) compared to control cells (4,831 ± 1,600) (Supplementary Fig. 4a). Focusing
127 on peaks shared by all four patients or three controls, we identified 1,396 gained peaks
128 exclusive to patients and only 88 peaks unique to controls (Fig. 3a; Supplementary Data 5).
129 Gene annotation revealed that H3K9me2 peaks spread mainly across intergenic and intronic
130 regions in both patient and control cells (Fig. 3b). However, when compared to the genome
131 using Genome Association Test, only a small significant enrichment of the mark at promoters
132 and 1-5kb regions in patient cells (Supplementary Fig. 4b). Biological processes associated with
133 the nearest promoters gaining H3K9me2 in patient cells did not show enrichment in immune
134 pathway genes or IRF/NFκB transcription factors (Suppmentary Data 6). Moreover, there was
135 no significant difference between patients and controls in the expression of H3K9me2-linked
136 genes (Supplementary Fig. 4c), and no correlation was identified between H3K9me2
137 concentration at the promoter level and gene expression (Supplementary Fig. 4d). Finally,
138 there was no enrichment of H3K9me2 reads at peaks showing either decreased or increased
139 accessibility (supplementary Fig. 4e), suggesting that H3K9me2 increase in CMML patients is
140 not directly linked to chromatin accessibility and gene expression.

141 Since H3K9me2 is also known to repress TEs[25,26], we analyzed CUT&Tag data by considering
142 all mapping reads, either unique and multiple, that mapped without mismatch, and we
143 randomly assigned them at one of their best possible positions in the genome, as described[11].
144 This analysis identified a pronounced enrichment of H3K9me2 at TEs relative to genes in
145 patients, with 13,364 TEs among H3K9me2-bound peaks in CMML cells, compared to 255 in
146 control cells (Fig. 3c; Supplementary Fig. 4f). Enrichment of TEs in patient and control peaks
147 was performed using a permutation test, counting peaks that intersected with any TE
148 belonging to a given TE class in CMML unique (gained) and control unique (lost) peaks and in
149 1000 times an equal number of peaks randomly chosen. This revealed that H3K9me2 peaks
150 gained in patient cells were significantly enriched for all TE classes (Fig. 3d; Supplementary
151 4g). In contrast, ERVs and SINEs were under-represented in lost peaks. The distribution of
152 H3K9me2 among TE classes showed that the proportion of ERVs was greater in peaks gained
153 than in peaks lost, while LINEs were overrepresented among TE lost (Fig. 3e). Overall, these
154 results highlight that the profound chromatin remodeling detected in CMML $CD34^+$ cells
155 involves an enrichment of H3K9me2 at TEs.
156
157 **The HMA and G9A/GLP inhibitor combination reduces CMML HSPC clonogenicity**
158 Recent data have shown that HMAs, when used in various pathological contexts, can act
159 through the reactivation of TEs[16,17], ultimately triggering the activation of IFN-I and NF-κB
160 pathways. Our initial results led us to speculate that deregulated G9A/GLP methyltransferases
161 and histone marks could interfere with CMML cell response to HMAs. To test this hypothesis,
162 CMML and healthy donor $CD34^+$ cells were treated *ex vivo* with the G9A/GLP inhibitor
163 UNC0638, the HMA decitabine (DAC) and their combination, then seeded in methylcellulose
164 for 14 days (Fig. 4a). Since H3K9me2 has been shown to bind to demethylated regions where

165 it can then reinstall DNA methylation[26,27], we added UNC0638 2 days after DAC. Dose-
166 response experiments demonstrated that each compound alone had a modest impact on
167 colony formation by patient cells, with 33% and 6% decrease observed at the highest dose of
168 DAC (80 nM) and UNC0638 (2 µM), respectively. In contrast, the combination of DAC and
169 UNC0638, even at low doses, significantly reduced the clonogenicity of these cells (Fig. 4b).
170 Using the Chou-Talalay method[28], a synergistic effect was observed under all conditions (Fig.
171 4c and d). Consistent with the low expression of G9A/GLP in these cells, no synergy between
172 DAC and UNC0638 on their clonogenicity was detected (Supplementary Fig. 5a). Although the
173 highest dose of DAC showed some toxicity on healthy cells, CMML leukemic cells were much
174 more sensitive to the DAC/UNC0638 combination, with the highest doses decreasing by 80%
175 and 20% the number of colonies formed by CD34+ cells from patients and control cells,
176 respectively.

177 Subsequent experiments were performed with 10 nM DAC followed by 1 µM UNC0638. A
178 significant reduction in global DNA methylation level was detected by ELISA after 2 days of
179 DAC, which was maintained at day 4, either alone or combined with UNC0638, while UNC0638
180 alone had no effect on DNA methylation (Supplementary Fig. 5b and c). The level of H3K9me2,
181 measured by immunofluorescence, remained unchanged after 2 days of culture in the
182 presence of DAC alone (Supplementary Fig. 5d), while it was markedly reduced by UNC0638
183 (Supplementary Fig. 5e). These experiments validated the proper functioning of the tested
184 drugs.

185 In the absence of treatment, the numbers of colonies formed by $CD34^+$ cells were comparable
186 between control and patient cells (Fig. 4e). Treatment with DAC+UNC0638 inhibited the
187 clonogenicity of 26 out of 28 tested CMML $CD34^+$ cells and reduced the colony size while each

188 inhibitor alone had a weaker (DAC) or no (UNC0638) effect (Fig. 4f; Supplementary Fig. 6a and
189 b). Again, none of these treatments affected the growth of control $CD34^+$ cells (Fig. 4g,
190 Supplementary Fig. 6a). Similar results were obtained with the combination of another HMA,
191 5-Azacytidine (AZA) combined with UNC0638, and with another G9A/GLP inhibitor, UNC0642,
192 combined with DAC (Supplementary Fig. 6c-f). Finally, CM-272, a dual inhibitor of DNMT1 and
193 G9A/GLP[29], specifically reduced the clonogenicity of CMML but not control $CD34^+$ cells (Fig.
194 4h and i).

195 To more precisely identify the cell population targeted by the combination, $CD34^+$ cells were
196 enriched in $CD34^+CD38^-CD90^+$ (HSC-enriched, referred to as stem cells) and $CD34^+CD38^-CD90^-$
197 (progenitor-enriched, referred to as progenitors) cells. We functionally assessed how the
198 inhibitors affected the cell clonogenic potential by testing their capacity to serially replate in
199 methylcellulose over 3 passages after treatment at day 2 and 4 of the culture (Fig. 5a). In the
200 absence of treatment, at all three passages, the number of colonies formed by control and
201 patient stem cells was not significantly different (Supplementary Fig. 7a and b). The
202 DAC/UNC0638 combination triggered a drastic reduction in the number and size of colonies
203 formed by both CMML stem cells and CMML progenitors (Fig. 5b and Fupplementary Fig. 7b
204 and c). DAC alone slightly decreased the size of the colonies generated by CMML progenitors
205 (Supplementary 7b) and, starting from P2, significantly reduced their number, while having no
206 effect on the stem cell-enriched population (Fig. 5b). Measuring the cumulative clonogenic
207 potential at P2, which considers both the number of colonies and their size[30], confirmed the
208 strong effect of the combination on both stem cells and progenitors while DAC affects in
209 priority the latter populations (Fig. 5c). None of the treatments affected colony formation by
210 stem cells or progenitors from controls (Supplementary Fig. 7c and d).

211 We further explored drug effects in single-cell liquid culture experiments for 14 days (Fig. 5d),
212 measuring cell viability (number of wells with at least one cell) and proliferation (total number
213 of cells in wells with at least one cell). In the absence of treatment, viability and expansion of
214 both stem cells and progenitors were similar in control and patient samples (Supplementary
215 Fig. 8a and b). However, the colony size formed by CMML cells was larger than those of
216 controls (Supplementary Fig. 8c). The combination reduced the viability and expansion of both
217 patient stem cells and progenitors (Fig. 5e-g). DAC treatment alone targeted patient
218 progenitors only, UNC0638 alone had no effect, and none of the treatments impaired the
219 viability and proliferation of control stem cells and progenitors (Supplementary Fig. 8d-f).

220 We subsequently interrogated the ability of the drug combination to selectively eliminate
221 leukemic cells by performing Sanger sequencing of pre-identified mutated genes
222 (Supplementary Table 2) in colonies grown from $CD34^+$ cells in methylcellulose and from
223 $CD34^+CD38^-CD90^+$ cells cultured at one cell per well for 14 days, focusing on somatic mutations
224 with a variant allele frequency (VAF) of 30% or more. Detecting mutations with the highest
225 VAF likely captures the primary events and major clones, as previous studies demonstrated
226 that mutations accumulate almost linearly in CMML stem and progenitor cells, with limited
227 branching events and early clonal dominance[2]. In line with previous findings[2], a minority of
228 wild-type cells (ranging from 0 to 40%) were found in untreated conditions (Fig. 6). The lack
229 of detection of wild-type cells in patient #3564 could be due to an overrepresentation of
230 mutated clones in methylcellulose[2] and the limited number of clones analyzed. While DAC and
231 UNC0638 showed limited effects when tested alone, the combination drastically reduced the
232 proportion of mutated clones in all patients (Fig. 6). In patients #3459 and #3562, with
233 mutations in *TET2* and *KRAS*, respectively, the major clones specifically and completely
234 disappeared. Patients #3480 (harboring clones with 0, 1, or 2 mutations) and #3564 (harboring

235 clones with 1, 2, or 3 mutations), showed increased proportions of non-mutated cells, along
236 with reduction in the most mutated clones carrying 2 or 3 mutations. UNC0638 alone slightly
237 increased the proportion of clones or colonies without any mutation (patients #3459 and
238 #3562) or harboring 1 vs. 2 mutations. DAC alone tended to favor the growth of clones
239 harboring mutations (patients #3459 and #3562) or the most mutated clones (increased size
240 of clones with 3 mutations from 59 to 78% in patient #3564). Altogether, these results show
241 that DAC and UNC0638 demonstrate a synergistic and specific impact on leukemic cells while
242 preserving wild-type cells.

243 **The HMA and G9A/GLP inhibitor combination increases TE expression in CMML CD34$^+$ HSPCs**

244 To assess the impact of DAC and UNC0638 on TE expression, we performed RNA-seq analysis
245 on CMML CD34$^+$ cells (n=4 patients) treated in liquid culture with or without DAC and/or
246 UNC0638 (Fig. 7a). Cells were harvested at day 4. At that time, the number of cells was not
247 significantly different between treated and non-treated conditions (Supplementary Fig. 9a).
248 Multimapping analysis of RNA-seq data revealed 340 differentially expressed TE families
249 ($p<0.05$), all exhibiting increased expression after treatment with the DAC/UNC0638
250 combination compared to untreated cells (Fig. 7b; Supplementary Data 7). In contrast, only
251 two differential TE families were identified after 4 days of treatment with either DAC or UNC
252 alone (Supplementary Fig. 9b and c). Upon DAC/UNC0638 combination, ERVs and DNA
253 transposons accounted for 43% and 32% of differentially expressed TEs, respectively (Fig. 7c).
254 Notably, ERV retrotransposons showed significant enrichment compared to LINEs and DNA
255 transposons (Fig. 7d). Comparative analysis of these deregulated TEs across all culture
256 conditions revealed that DAC and UNC0638 alone elevated the expression of ERV and DNA
257 transposons compared to untreated cells, with the combination synergistically increasing the

258 expression of ERVs, DNA and LINEs (Fig. 7e; Supplementary 9d). None of the treatments
259 affected SINE expression.

260 Focusing on ERVs that displayed the most significant differential expression upon
261 DAC/UNC0638 treatment, we conducted a loci-based quantification, as described in our
262 previous work[31], incorporating four additional patient samples. We identified 2,120
263 differentially expressed ERV loci ($p<0.05$, FC 1.5) between untreated and DAC/UNC0638
264 conditions, most of them (97%) upregulated (Fig. 7e and f; Supplementary Data 8). Confirming
265 the results above, the impact of DAC or UNC0638 treatment alone was notably weaker,
266 resulting in 120 and 122 differentially regulated ERV loci, respectively, compared to non-
267 treated condition (Fig. 7f and g). A majority of the ERVs induced by the combination
268 (1991/2056) were specific to this condition, whereas either treatment alone upregulated very
269 few specific ERVs (10% and 20% for UNC0638 and DAC, respectively). Conversely, differentially
270 downregulated loci were largely specific to each condition (48/58 and 43/43 of the ERVs
271 downregulated by UNC0638 or DAC alone). Focusing on ERVs differentially expressed in all
272 conditions compared with untreated cells, the vast majority of loci exhibited a synergistically
273 higher expression level in cells treated with the combination than in DAC or UNC0638
274 treatment alone (Fig. 7h). RT-qPCR experiments targeting ERV family members deregulated
275 by the combination further validated their greater or synergistic induction after 4 days of
276 treatment with DAC/UNC0648 compared to either inhibitor alone (Fig. 7i). Together, these
277 results indicate that the HMA and G9A/GLP inhibitor combination, but not each inhibitor
278 alone, induces a significant and rapid derepression of TEs, particularly ERVs, in CMML $CD34^+$
279 cells.

280 **The DAC/UNC0638 combination reactivates viral and inflammatory pathways in CMML cells**

281 ERVs can generate double-stranded RNAs (dsRNAs) that are recognized by antiviral pattern
282 sensors, leading to IFN-I production and activation of the IFN/NFκB pathway—a process
283 known as viral mimicry, which exhibits an anti-tumoral effect[13,16,17]. Analysis of coding gene
284 expression revealed 3,227 DEGs ($p<0.05$, FC 1.2), of which 2,914 (90%) are positively and 313
285 (10%) are negatively expressed in DAC/UNC0638 treated compared with untreated $CD34^+$
286 cells (Fig. 8a and b; Supplementary Data 9). Treatment with DAC or UNC0638 alone induced
287 only 187 and 158 DEGs, respectively, with 56% and 53% being overexpressed, and 44% and
288 47% being downregulated. GSEA revealed that genes upregulated by the DAC/UNC0638
289 combination were enriched for IFN, NFκB, and other inflammatory pathways, TP53, and
290 apoptosis. In contrast, downregulated genes included those associated with DNA and histone
291 methylation, transcription, and cell proliferation pathways (Fig. 8c and d and Supplementary
292 10a-d). No specific gene sets were found to be enriched in cells treated with DAC or UNC0638
293 alone. Gene Set Variation Analysis (GSVA) revealed that the majority of IFN signaling and IFN
294 production signatures were positively enriched as compared with any individual treatment
295 (Fig. 8e). RT-qPCR experiments showed that the combination significantly increased the
296 expression of *IFNB1* mRNA, encoding IFN-β, and TFs such as *IRF9* and *IRF7* involved in IFN
297 signaling (Fig. 8f), confirming RNA-seq results. Altogether, these data demonstrate that TE
298 derepression induced by the combined treatment correlates with the reactivation of viral and
299 inflammatory pathways in $CD34^+$ cells from CMML patients.

300 **The induction of IFN signaling by the combination is essential for eliminating CMML HSPCs**

301 We further examined whether IFN signaling is dysregulated at the protein level.
302 Immunofluorescence analysis demonstrated increased levels of key proteins involved in IFN-I
303 production (IRF3 and IRF7) and IFN signaling (STAT1) in $CD34^+$ cells from CMML patients after
304 4 days of culture with DAC/UNC0638, compared to untreated cells (68-fold, 50-fold, and 3-

305 fold increase, respectively) (Fig. 9a-c). While HMA treatment alone significantly increased IRF7
306 and STAT1 protein levels, the combination induced a much stronger response. Notably, only
307 the combination led to a substantial increase in the phosphorylated form of STAT1 (pSTAT1)
308 (98-fold compared to untreated), indicating the activation of IFN signaling after 4 days of
309 culture (Fig. 9d). In control cells, only a modest increase in IRF3 was observed upon treatment
310 with the combination (1.5-fold), and this increase was notably lower compared to that
311 observed in patients (68-fold) (Supplementary Fig. 11a-d). These findings further underscore
312 the specific and potent activation of IFN signaling achieved by the combination treatment in
313 CMML $CD34^+$ cells.

314 To investigate the potential involvement of ERVs in activating IFN signaling, we assessed
315 dsRNA formation using J2 antibody that specifically recognizes dsRNAs. The combination
316 treatment markedly increased dsRNA expression in patient $CD34^+$ cells, while having no
317 significant effect on control cells (Fig. 9e; Supplementary Fig. 11e). Consistent with its modest
318 impact on IRF7 and STAT1 expression, DAC alone showed a slight increase in dsRNA
319 expression, whereas UNC0638 alone had no observable effect (Fig. 9e). We then explored
320 whether cell death induced by the combination could be related to IFN-I signaling activation
321 by treating $CD34^+$ cells with the DAC/UNC0638 combination in the presence or absence of an
322 antibody blocking IFNAR2 (IFN-I receptor) before being cultured in methylcellulose (Fig. 10a).
323 Blocking IFNAR2 partially restored the clonogenic capacity of CMML $CD34^+$ cells in the
324 presence of DAC/UNC0638 (Fig. 10b and c). This finding highlights the contribution of the
325 antiviral response of malignant cells to the efficacy of the DAC/UNC0638 combination.

326

327 **Discussion**

328 This study reports the first comprehensive characterization of chromatin and transcriptomic
329 changes in CMML compared to age-matched healthy donor CD34$^+$ cells upon *ex vivo* exposure
330 to HMAs. We demonstrate that CMML CD34$^+$ cells, regardless of their mutation pattern,
331 exhibit repression of immune and age-associated transcripts, coupled with an increase in the
332 repressive H3K9me2 mark, predominantly at TEs. This chromatin context may protect them
333 from both TE activation[9,14] and the highly inflammatory environment that characterize aging,
334 and promote their expansion[18,19,22,32,33]. Reactivation of TEs and TE-induced innate immune
335 response, achieved through a combination of HMAs and G9A/GLP inhibitors, appears to
336 decrease the fitness of mutated cells compared to residual wild-type cells (Fig. 10c). This
337 discovery opens up new therapeutic avenues for treating this severe myeloid malignancy.

338 The depicted downregulation of proinflammatory genes in CMML compared to age-matched
339 healthy donor CD34$^+$ cells contrasts with the proinflammatory transcriptome of CMML
340 monocytes[32] and the increased level of various inflammatory cytokines in peripheral blood
341 plasma of CMML patients[33-35]. HSC aging is associated with an increased expression of
342 proinflammatory genes[18,19,22,36] likely indicative of the cumulative impact of infections and
343 various stresses over the lifespan, and chronic inflammation promotes premature HSC aging
344 in mice[37]. Recent findings highlight chromatin accessibility changes in aged mouse HSCs, with
345 open regions notably enriched for TF activated in response to cytokine signals and
346 inflammation, such as the JAK-STAT pathway. These open regions exhibit a correlation with
347 gene expression levels[18]. Senescent human HSPCs exhibit heightened expression of TEs and
348 inflammatory genes[38]. The presence of enriched NFκB and IRF motifs in peaks displaying
349 reduced chromatin accessibility suggests that CMML HSPCs may have a diminished capacity

350 to respond to this highly inflammatory milieu. This might protect them from the deleterious
351 effects of aging and inflammation when compared to wild-type CD34$^+$ cells, a difference that
352 should contribute to the expansion of the leukemic clone. Supporting this hypothesis, we
353 observed a decline in senescence and aging signatures in CD34$^+$ cells from CMML compared
354 to those from aged healthy donors. Our recent results also indicate that dysplastic
355 granulocytes generated by the CMML clone produce high levels of CXCL8 that inhibits the *ex*
356 *vivo* growth of wild-type CD34$^+$ cells while having limited effects on mutated CD34$^+$ CMML
357 cells, thereby promoting leukemic clone expansion[39]. Consistent with these findings, studies
358 in zebrafish and humans have reported that the muted inflammatory response of mutant
359 HSCs, compared to wild-type HSCs in the same samples, renders them more resistant to
360 inflammation and aging, facilitating their selection[40,41]. These results suggest that epigenetic
361 drugs that enable the reactivation of inflammatory/antiviral responses in CMML HSCs may
362 break out such vicious circle in CMML as well as other age-associated malignancies.

363 In a previous work, we showed that HMAs could restore a balanced hematopoiesis in CMML
364 patients without decreasing the mutation VAF nor preventing clonal evolution, indicating that
365 these compounds could not eradicate the malignant clone[4]. Similar observations were made
366 in MDS patients treated with 5-AZA[42,43]. An additional observation is provided by our
367 experiments indicating that HMAs selectively target progenitors while having no detected
368 effect on stem cells in both liquid culture and methylcellulose assays. Even more, DAC appears
369 to slightly promote the growth of the most mutated cells, which could explain why CD34$^+$ cells
370 from HMA-responsive MDS patients were observed to be enriched in progenitor cells as
371 compared with non-responders[42,43]. Similarly, HMAs were reported to predominantly target
372 granulo-monocytic progenitors in high-grade MDS and acute myeloid leukemia (AML) [43]. The
373 high expression of cell cycle-associated genes depicted in CMML CD34$^+$ cells who respond to

374 HMAs may promote their incorporation in nucleic acids[44]. The lower expansion of stem cells
375 compared to progenitors (mean fold expansion of 20.34 +/- 0.34 and 32.26 +/- 0.98 in 8 days,
376 respectively) may also contribute to the greater sensitivity of progenitors to HMAs.
377 Alternatively, differences in DNA and histone methylation, expression of genes encoding RNA
378 helicases and autophagy genes[45] might exist between CMML progenitor and stem cells.

379 Our findings indicate that DAC as a single agent is an inefficient inducer of either TE expression
380 or inflammatory / IFN signaling in CMML $CD34^+$ cells *ex vivo*. The role of these events in HMA
381 activity in myeloid malignancies remains controversial. 5-AZA was initially reported to
382 upregulate the expression of some ERVs in primary $CD34^+$ cells collected from MDS patients[46].
383 Overexpression of TEs in DNMT3A-mutant AML cells renders them more sensitive to 5-AZA
384 via viral mimicry response[47]. An increased transcription of evolutionary young TEs with an
385 activation of innate immune responses was depicted in some 5-AZA-responders[48] but not
386 validated in others[49]. These discrepancies could be related to the heterogeneity of the studied
387 cohorts with diverse diseases[48,49] and genetic backgrounds[50,51] as well as methodological
388 issues.

389 While TEs are commonly recognized for their tumor-promoting functions, recent studies have
390 suggested that RTEs, including active LINE-1 and ERVs, have been evolutionarily selected for
391 their tumor-suppressing function through their ability to induce viral mimicry and/or p53
392 activation[52]. Accordingly, TE transcription is commonly suppressed along tumor progression,
393 for example from low-grade to high grade MDS, then a full-blown AML[45], where a low
394 repeat/gene expression ratio correlates with a poor outcome[53]. This is associated with the
395 inactivation of innate immune pathways, including IFN and NFκB signatures, potentially
396 contributing to the immune evasion mechanism observed in this pathology. One study also

397 reported that CMML and MDS CD34$^+$ cells expressed lower levels of TEs than healthy donor
398 cells[49]. Epigenetic mechanisms that were shown to contribute to TE repression in myeloid
399 malignancies include the H3K9 methyltransferase SETDB1[54] and the epigenetic repressor
400 complex HUSH whose component MMP8 mediates LINE-1 element repression[55]. The decrease
401 in H3K9me3 observed in CMML CD34$^+$ cells suggests this mark may not be involved in the
402 repression of TEs and TE-induced innate immune response in these cells. The sharp increase
403 in H3K9me2 and G9A/GLP methyltransferase expression, which was detected in CMML cells
404 may compensate for H3K9me3 loss. A similar increase in H3K9me2 expression was shown to
405 prevent type I IFN pathway activation and immune gene expression in AML cell lines[24]. Our
406 CUT&Tag analysis show that H3K9me2 is mainly located at TEs and did not indicate a direct
407 inhibitory effect of H3K9me2 on immune gene expression. In addition, the G9A/GLP inhibitor
408 UNC0638 alone did not induce IFN/inflammatory signaling in CMML CD34$^+$ cells. G9A interacts
409 with DNMT1 and recruits DNMT3A/B through MPP8 to promote the compaction of chromatin
410 in H3K9me2-marked regions[56]. In embryonic stem cells, loss of H3K9me2 was shown
411 insufficient to generate a global DNA demethylation[57]. In HSPCs, the H3K9me2 mark is
412 detected preferentially in demethylated regions and participates in global changes in
413 chromatin structure during myeloid differentiation[27]. This could explain a synergistic effect of
414 G9A/GLP inhibition with HMAs on TE expression.

415 Besides controlling TE expression, G9A/GLP has been shown to play a role in AML leukemic
416 cell stemness[58]. Altogether, the present study designates G9A/GLP inhibition as a promising
417 strategy to specifically target leukemic stem cells in CMML. Even if the combination slightly
418 impacted control cells *in vitro,* its effect was far more efficient on mutated cells, as shown by
419 the selective eliminatation of mutated leukemic HSCs while preserving wild-type cells in the
420 same patient CMML sample (Fig. 6). Unfortunately, our attempts to explore the ability of

421 HMAs combined to the current G9A/GLP inhibitors to eradicate leukemic stem cells in patient-
422 derived xenografts established in mice was precluded by the toxic side effects of the
423 combination compounds. This could be due to small effect of the combination on healthy
424 murine progenitors. Less-toxic direct inhibitors or alternative indirect approaches will be
425 needed to validate the merit of this therapeutic approach.

426

427 **Materials and methods**

428 **Patient and healthy donor samples and processing**

429 The study was carried out on patients diagnosed with CMML, before any treatment according
430 to the 2016 iteration of the WHO classification (Supplementary Table 1). Patient BM samples
431 were obtained as part of a BM assessment of the disease carried out in one of the hematology
432 department affiliated to the Groupe Francophone des Myélodysplasies (GFM). Informed
433 consents were obtained in agreement with Ile-de-France ethics committee (MYELOMONO
434 cohort, DC-2014-2091). Mutations were detected in patients' monocyte DNA by next
435 generation sequencing (NGS) using a myeloid panel, as previously described [4]. Age-matched
436 healthy donor BM samples were obtained from femoral heads from individuals who had
437 undergone surgery to treat mechanical osteoarthritis, thanks to the banque de tissus osseux,
438 (Hôpital Cochin). Cord blood was obtained from Unité de Thérapie Cellulaire, CRB-Banque de
439 Sang de Cordon, (AP-HP Hôpital Saint-Louis, Paris) - Authorization no.: AC-2022-5325.
440 Informed consent was obtained from all donors, in accordance with the Declaration of
441 Helsinki. Samples were collected sequentially and cell culture were performed directly on
442 arrival without prior freezing / thawing. Patient samples were collected by BM puncture with
443 EDTA aspiration. BM cells from healthy elderly subjects were obtained by flushing the femoral
444 head in PBS (Gibco). After washing and resuspension in PBS, the cells were filtered on 70 µM
445 nylon mesh. HSPCs were obtained from mononuclear cells sorted on a Ficoll gradient (Pancoll,
446 PAN-Biotech) and isolated by positive magnetic cell sorting performed on CD34 marker
447 expression following the manufacturer's instructions (AutoMACS ProSeparator, Miltenyi
448 Biotech). For sorting stem cell-enriched ($CD34^+CD38^-CD90^+$) and progenitor-enriched
449 ($CD34^+CD38^-CD90^-$) populations, cells were further stained with CD38-PE-Cy7 (BD Biosciences;

450 clone HB-7), CD90-FITC (Sony Biotechnologies; clone HIT2) and sorted on ARIA fusion cell
451 sorter.

452 **Cell cultures and treatments**

453 Freshly isolated human HSPCs were plated at 200,000 cells/ml and cultured in IMDM medium
454 supplemented with 25% BIT9500 (StemCell Technologies), 1% penicillin/streptomycin (P/S),
455 containing the following cytokines (all from Miltenyi Biotech): FTL3-Ligand (FTL3-L, 100ng/µL),
456 Thrombopoietin (THPO, 100ng/µL), stem cell factor (SCF, 60ng/µL) and interleukin 3 (IL3,
457 10ng/µL), at 37°C, 20% O2, 5% CO2. For treatments, decitabine (DAC, Sigma Aldrich), or 5-
458 Azacytidine (AZA, Sigma Aldrich) were added at the start of the cultures (day 0) and again on
459 day 1. G9A/GLP inhibitor (UNC0638 or UNC0642, MedChem) was added once on day 2. The
460 dual DNMT/G9A inhibitor, CM-272 (Axon Medchem) was added on day 0 and again 48h later
461 and the cells were directly seeded in methylcellulose.

462 **Single cell colony and CFU assays**

463 Single human or mouse HSCs/HSPCs were FACS-sorted into individual wells of round-bottom
464 96 well plates and cultured in the presence or absence of inhibitors. At different times starting
465 day one, each well was checked manually for the the presence of cells. For CFU assays, 300
466 $CD34^{+}$ or 100 $CD34^{+}CD38^{-}CD90^{-/+}$ treated or not with the inhibitors were seeded in duplicate
467 in 24-well plates containing 300µl of methylcellulose (H4230, StemCell), supplemented with
468 1% P/S (ThermoFischer Scientific), FLT3-L (25ng/µL), THPO (25ng/µL), SCF (60ng/µL), IL3
469 (10ng/mL), EPO (2 units), GM-CSF (10ng/mL). Colonies were counted after 14 days of culture.
470 The mean size of the colonies was estimated by harvesting them and counting the total
471 number of cells in the well. For replating assays, 5000 cells were replated in methylcellulose
472 in the same medium. This process was repeated twice. The cumulative CFU potential that

473 takes into account both the number of CFUs and their size was calculated at passage 2
474 described [30].

475 **Gene mutation screening in colonies**

476 Mutations with VAF ≥ 30% were analyzed after *in vitro* treatment (Supplementary Table 2).
477 Colonies from $CD34^+$ or $CD34^+CD38^-CD90^+$ cells grown in methylcellulose or in single cell liquid
478 cultures, respectively, in the presence or absence of DAC and/or UNC0638, were picked up
479 individually after 14 days, washed and stored at -80°C as dry pellets. Cells were lysed with a
480 solution containing proteinase K (0.1 mg/mL, Fisher Scientific), 2% Tween-20 (Sigma-Aldrich)
481 and incubated for 1 h at 65°C followed by 15 min at 95°C. DNA was amplified by PCR using the
482 Q5 High-Fidelity DNA polymerase kit (New England BioLabs) and primers designed around the
483 mutations (Supplementary Table 3). Amplicon sizes were verified by migrating the amplified
484 DNA sample onto a 1.8% agarose gel. The amplified DNA fragments were analyzed by Sanger
485 sequencing (Eurofins Genomics, Ebersberg, Germany). 8-12 clones were tested per condition.

486 **ELISA for DNA methylation**

487 Cell lysis and extraction of genomic DNA from dry pellets were performed using the
488 NucleoSpin Tissue XS kit (Macherey-Nagel). Genomic DNA quality and quantity were
489 measured using the NanoDrop (ND-1000, Marshall Scientific). Global DNA methylation was
490 studied using the global DNA methylation assay kit - LINE-1 (Active Motif) according to the
491 manufacturer's instructions.

492 **Immunofluorescence**

493 5000 human and murine HSPCs/HSCs were fixed with 4% paraformaldehyde (PFA) for 10 min
494 at RT and centrifuged (Tharmac) on poly-L-Lysine slides (Fisher Scientific).
495 Immunofluorescence was performed as described previously[11,14]. The primary antibodies used

496 are listed in Supplementary Table 4. Detection was performed using anti-rabbit secondary
497 antibody coupled to Alexa-Fluor 488 or anti-mouse coupled to Alexa-Fluor-555. All slides were
498 viewed under a TCS SPE confocal microscope (Leica). Images were analyzed and fluorescence
499 intensities calculated using ImageJ software, as described[11,14].

500 **RNA purification and quantitative RT-PCR**

501 50,000 - 150,000 cells were lysed in Tri-Reagent solution (Zymo Research) and stored at -80°C
502 until use. Total RNA was extracted using the Direct-Zol RNA microprep kit (Zymo Research).
503 RNAs were reverse transcribed using the EZ DNAse VILO IV kit (Invitrogen). 1.25 µL of cDNA
504 was pre-amplified for 15-18 cycles in a multiplex reaction using Preamp Master-Mix solution
505 (ref. 100-5580, Fluidigm) and primer mix (200 µM of each primer; supplemental Table S3), as
506 described[11]. Quantitative PCR (qPCR) was performed using LUNA Universal qPCR Master Mix
507 (New England Biolabs) on the 7500 real-time PCR machine (Applied Biosystems). Data were
508 normalized with the mean expression of household genes (HPRT, Tubulin, GUS, PPIA and / or
509 RPL32).

510 **ATAC-seq and data processing**

511 100,000 freshly isolated $CD34^+$ cells were processed with the ATAC-seq kit (Active Motif).
512 Transposed DNA fragments were amplified 10-fold by PCR using adapters supplied by the kit.
513 PCR purification was carried out using MinElute PCR Purification Kit (Qiagen, 28004) to remove
514 remaining primers and large fragments. The quantity and quality of the libraries were assessed
515 on Agilent 2100 Bioanalyzer (Agilent Technologies 50567-4626). Sequencing of the libraries
516 was performed on the NovaSeq-6000 at Gustave Roussy (Illumina; 50 bp paired-end reads).
517 ATAC-seq data were processed essentially as described[15]. Read quality was assessed using
518 Fastqc[59] (v0.11.9) and MultiQC[60]. Bowtie2[61] (v.2.3.4.1) using the «--very-sensitive» parameter

519 was used for aligning ATAC-seq reads to the human genome version GRCh38/hg38 and
520 Samtools (v.1.7) for data filtering and file format conversion. Duplicate reads were removed
521 with Picard tool - MarkDuplicates (http://broadinstitute.github.io/picard), blacklist regions,
522 chrM and Y were removed with BEDtools intersect and grep -v respectively before peak
523 calling. All filtered.bam files were converted to bedgraphs using the DeepTools bamCoverage
524 subcomm and, with the reads per kilobase of transcript, per million mapped reads (RPKM)
525 normalization method. MACS2 (v.2.1.1)[62] algorithm was used for peak identification (Q-value
526 cut-off = 0.01). Gained and lost peaks were identified from the narrow peaks in two steps.
527 First, the peak lists from control and CMML patients were merged separately with the
528 subcommands cat and mergeBed to obtain consensus peaks. Second, with intersectBed and
529 the parameters --a <consensus peaks> --b <narrow peaks> --wa --u and subsequently --v, we
530 compare and subtract them, to take the gained and lost peaks for each group. The reads of
531 these consensus peaks were counted and a statistical model based on edgeR[63] was used to
532 identify the significantly differential peaks. To identify the common peaks between patients
533 or controls, DESeq which uses the Negative Binomial distribution to compute a P value and a
534 fold change for each estimated peak was used. Peaks highly enriched in comparison to the
535 rest were considered gained. Annotation of peaks to genes (100 kb upstream and 25 kb
536 downstream from the TSS) and genomic distribution of accessible regions identified by MACS2
537 was performed using BEDTools and the -closestBed and -intersectBed subcommands,
538 respectively. Clustering of regions was generated with the ComputeMatrix function of
539 DeepTools, using the reference point --referencePoint center -b 2500 -a 2500 -R <bed files> -
540 S <bigwig files> as parameters. The function plotHeatmap from the same package was used
541 for displaying the average profiles heat map. Differentially accessible chromatin regions were

542 scanned for enriched short-sequence motifs using HOMER software [64] with
543 "findMotifsGenome.pl" command.
544
545 **RNA-sequencing and data processing**
546 RNA quality was checked on the Agilent Bioanalyzer and quantified. 100-250 pg of total RNA
547 extracted from CD34$^+$ cells were used to prepare cDNA libraries, as described[11], using the
548 SMARTer Ultra Low Input RNA Kit for Sequencing - v3 or -SMARTer Stranded Total RNA-seq kit
549 v3, according to the manufacturer's recommendations (Takara). Libraries were sequenced in
550 (2 x 100bp) on the NovaSeq-6000 (Illumina). Read quality was assessed with Fastqc v0.11.9,
551 and corrected with Fastqp[59] v0.23.1. Alignments were performed with STAR (v2.7.10b) on
552 GRCh38 human genome reference. Mapped reads underwent filtration to retain only those
553 associated with regular chromosomes (1-23, XY) and the remaining reads were sorted and
554 indexed. Raw count table were generated with FeatureCounts (package subread, v2.0.1).
555 Transcript expression levels were aggregated in gene expression levels using tximport
556 Bioconductor package v1.13.16. For the CMML versus controls, a batch effect correction was
557 first done using ComBat-seq function of the sva package, before subsequent DESeq2
558 analysis[65]. PCA analysis was performed with DESeq2, after regularized log transformation of
559 gene counts using default parameters. Pathway analysis were performed and plotted on R
560 using msigdbr (7.5.1), and clusterProfiler (4.2.2 or 4.6) or the GSEA app of MSigDB. GSEA
561 analyses of CMML vs. controls cells were performed and genes pre-ranked on the statistical
562 result of the differential analysis, and pathways were sorted on their normalized enrichment
563 score (NES) before plotting.
564 Multimapping and expression of TE families was analyzed with TEtranscript (v 2.2.1)[66]. Paired-
565 end reads were aligned to GRCh38 genome using STAR (v2.7.11a) with these parameters: --

566 winAnchorMultimapNmax 100 --outFilterMismatchNmax 3 --alignEndsType EndToEnd --
567 alignIntronMax 1 --alignMatesGapMax 350. Differentially expressed TEs were identified using
568 the R (v4.1.2) package DESeq2(v1.3.4), with criteria including p-value < 0.05 and an absolute
569 value of log2(FC) > 0. ERV expression was quantified using a loci-based approach, as previously
570 described [31]. Briefly, RNA-seq reads were aligned to a custom transcriptome using bowtie2
571 v2.2.1 with custom parameters to retain multimapped reads (-k 100 --very-sensitive-local --
572 score-min "L,0,1.6"). The custom transcriptome consisted in the hg38 reference transcriptome
573 with 14,968 ERV transcriptional units compiled from RepeatMasker annotations [67]. ERV and
574 gene expression were then quantified using Telescope[67] and HTSeq 0.12.3[68], respectively. Raw
575 counts were concatenated and normalized independently for each dataset using DESeq2
576 v1.28.0 with variance stabilizing transformation. Differential expression analysis was
577 performed using DESeq2. Raw counts of ERVs and genes were merged and integrated into the
578 same DESeq object, using patient ID and condition as a covariate in the design formula to
579 account for data pairing (design = ~ patient_id + condition). For each comparison, the
580 untreated (NT) condition was considered as reference. Fold change were shrunk with the
581 ASHR method [69]. Union of differentially expressed coding genes or ERV were selected based
582 on a 1.5-fold change and pvalue < 0.05. IFN signatures were retrieved from The Molecular
583 Signatures Database (MSigDb). Individual enrichment scores were calculated from each
584 patient by single sample gene-set variation analysis (ssGSVA), and center-scaled.

585 **CUT&Tag and data processing**

586 CUT&Tag assays were performed using CUT&Tag-IT assay kit (Active Motif) on 50,000 $CD34^+$
587 cells, as described [11], using 0.5µg of H3K9me2 antibody (Abcam Ab1220). Sequencing of the
588 libraries was performed on the NovaSeq-6000 (Illumina; 2x 50 bp). CUT&Tag data were

589 processed and analyzed mostly as described[11]. Paired-end reads were aligned to GRCh37
590 genome using Bowtie2 (v2.4.1) with the following parameters: --end-to-end --very-sensitive -
591 -no-mixed --no-discordant --phred33 -I 10 -X 700. Duplicate reads were excluded using Picard
592 (v2.26.9). Reads aligned on regular chromosomes were retained and the aligned read quality
593 score was set to «0» using samtools (v1.13) to get both uniquely mapped and multimapped
594 reads. The Y chromosome was removed from the downstream analysis. The aligned reads
595 underwent two processing methods: 1) direct sorting and indexing BAM files using samtools
596 (v1.13), followed by peak calling with MACS2 (v2.2.7.1) with the specified parameters adapted
597 to broad marks: -B --broad --broad-cutoff 0.1 -f BAMPE -g hs --max-gap 2000 --min-length 200.
598 2) Downsampling BAM files to the minimum read count across BAM files, subsequent sorting,
599 and indexing using samtools (v1.13). Processed BAM files were then utilized for extracting
600 read counts within peaks. Subsequent downstream analysis was carried out using custom
601 scripts in R (v4.1.2). A matrix of counts for union peaks was generated using chromVAR
602 (v1.16.0) R package and differentially expressed peaks between CMML Patients and controls
603 were identified using the R (v4.1.2) package DESeq2(v1.3.4) , with criteria including an p-value
604 < 0.05 and an absolute value of log2(FC) > 0. Peaks consistently identified across all control or
605 patient biological replicates were kept for further analysis. Enrichment of TEs in peaks was
606 performed using a permutation test conducted independently for each TE class. A peak was
607 considered associated with a TE if there is at least 1 base pair overlap between them. Peaks
608 that intersected with any TE belonging to a given TE class were counted in CMML unique
609 (gained) and control unique (lost) peaks. An equal number of peaks were randomly chosen
610 from peaks that do not belong to any section of the Venn diagram, and the count of peaks
611 overlapping with the designated TE class was determined. This iterative process was repeated
612 1000 times to establish a null distribution for the number of peaks overlapping with the TEs.

613 Enrichment or depletion of the different classes of TEs was calculated as the log2 fold change
614 of the number of specific peaks overlapping with TEs in any TE class found in patient gained
615 or lost peaks over the median number of TEs of the same class in the randomly selected peaks.
616 The empirical p-value was calculated by dividing by 1000 the number of occurrences where
617 the permutation resulted in values exceeding the number of gained peaks overlapping the TE
618 class.

619 **Statistics and reproducibility**

620 Results were statistically evaluated by one-way or two-way ANOVA tests or paired and
621 unpaired t-tests using Prism GraphPad PrismTM software (GraphPad Software Inc., San Diego,
622 CA, USA). Graphs show mean and standard error to the mean (SEM). Values of $p<0.05$ are
623 considered statistically significant. The use of statistical test, the *p* value, the numbers of
624 samples and experiments are indicated in the respective Fig
625 ure legends.

626 **Data availability**

627 All raw sequencing Fasq data for RNA-seq, CUT&tag and ATAC-seq presented in this paper will
628 be available through the European Genome-phenome Archive (EGA) under the accession
629 number EGAS50000000367. The data supporting the finduinds of these study are available in
630 Supplementary Data files 1 to 8 joined with the paper. All source data underlying the graphs
631 and charts presented in the main figures are provided in the Supplementary Data 9.

632 **Supplemental material**

633 Supplementary material includes 11 figures related to Figures 1 to 10, 4 tables and 10 Data
634 files.

635

636 **Acknowledgments**

637 We thank Thorsten Braun (Clinical Hematology Department, Hôpital Avicenne, Bobigny),
638 Céline Berthon (Clinical Hematology Department, University Hospital, Lille), Gabriel Etienne
639 (Clinical Hematology Department, University Hospital, Bordeaux), Pierre Fenaux (Hematology
640 Department, Saint-Louis Hospital, Paris) Christophe Willekens (Clinical Hematology
641 Department, Gustave Roussy Cancer Center, Villejuif) for providing patient samples; animal
642 facility, the Genomic and the Imaging and Cytometry Platforms of Gustave Roussy for
643 sequencing and cell sorting and confocal analysis, respectively and Dr. Louis Paré (Nantes
644 University, École Centrale Nantes) for RNA-seq analysis. This work was supported by INSERM
645 and grants from Ligue Nationale Contre le Cancer (LNCC, Equipe labellisée EL2020) and Institut
646 National du Cancer (PLBIO N°2020-095) to F.P. D.H. and A.P. are recipients of fellowship from
647 the Ministère de l'Enseignement Supérieur de la Recherche et de l'Innovation.

648 **Author contributions**

649 DH, AP MB, AI performed experiments, acquired and analyzed the results. RC, AiP, VA, SD, LL
650 performed bioinformatic analyses. ND performed next generation sequencing and analyzed
651 data. AR, DSB, ET analyzed data. SP, RI provided samples. MM processed samples. ES analyzed
652 data and wrote the manuscript. FPu designed and supervised the study, conducted
653 experiments, analyzed the results and wrote the manuscript.

654

655

656

657

658 **References**

659 1 Khoury, J. D. *et al.* The 5th edition of the World Health Organization Classification of
660 Haematolymphoid Tumours: Myeloid and Histiocytic/Dendritic Neoplasms. *Leukemia* **36**,
661 1703-1719 (2022). https://doi.org/10.1038/s41375-022-01613-1
662 2 Itzykson, R. *et al.* Clonal architecture of chronic myelomonocytic leukemias. *Blood* **121**, 2186-
663 2198 (2013). https://doi.org/10.1182/blood-2012-06-440347
664 3 Binder, M. *et al.* Oncogenic gene expression and epigenetic remodeling of cis-regulatory
665 elements in ASXL1-mutant chronic myelomonocytic leukemia. *Nature communications* **13**,
666 1434 (2022). https://doi.org/10.1038/s41467-022-29142-6
667 4 Merlevede, J. *et al.* Mutation allele burden remains unchanged in chronic myelomonocytic
668 leukaemia responding to hypomethylating agents. *Nature communications* **7**, 10767 (2016).
669 https://doi.org/10.1038/ncomms10767
670 5 Palomo, L. *et al.* DNA methylation profile in chronic myelomonocytic leukemia associates with
671 distinct clinical, biological and genetic features. *Epigenetics* **13**, 8-18 (2018).
672 https://doi.org/10.1080/15592294.2017.1405199
673 6 Solary, E. & Itzykson, R. How I treat chronic myelomonocytic leukemia. *Blood* **130**, 126-136
674 (2017). https://doi.org/10.1182/blood-2017-04-736421
675 7 Tsurumi, A. & Li, W. X. Global heterochromatin loss: a unifying theory of aging? *Epigenetics* **7**,
676 680-688 (2012). https://doi.org/10.4161/epi.20540
677 8 Zhang, W., Qu, J., Liu, G. H. & Belmonte, J. C. I. The ageing epigenome and its rejuvenation.
678 *Nature reviews. Molecular cell biology* **21**, 137-150 (2020). https://doi.org/10.1038/s41580-
679 019-0204-5
680 9 Djeghloul, D. *et al.* Age-Associated Decrease of the Histone Methyltransferase SUV39H1 in HSC
681 Perturbs Heterochromatin and B Lymphoid Differentiation. *Stem Cell Reports* **6**, 970-984
682 (2016). https://doi.org/10.1016/j.stemcr.2016.05.007
683 10 Keenan, C. R. *et al.* Extreme disruption of heterochromatin is required for accelerated
684 hematopoietic aging. *Blood* **135**, 2049-2058 (2020).
685 https://doi.org/10.1182/blood.2019002990
686 11 Pelinski, Y. *et al.* NF-kappaB signaling controls H3K9me3 levels at intronic LINE-1 and
687 hematopoietic stem cell genes in cis. *The Journal of experimental medicine* **219** (2022).
688 https://doi.org/10.1084/jem.20211356
689 12 Chuong, E. B., Elde, N. C. & Feschotte, C. Regulatory activities of transposable elements: from
690 conflicts to benefits. *Nature reviews. Genetics* **18**, 71-86 (2017).
691 https://doi.org/10.1038/nrg.2016.139
692 13 Gazquez-Gutierrez, A., Witteveldt, J., S, R. H. & Macias, S. Sensing of transposable elements by
693 the antiviral innate immune system. *RNA* **27**, 735-752 (2021).
694 https://doi.org/10.1261/rna.078721.121
695 14 Barbieri, D. *et al.* Thrombopoietin protects hematopoietic stem cells from retrotransposon-
696 mediated damage by promoting an antiviral response. *The Journal of experimental medicine*
697 **215**, 1463-1480 (2018). https://doi.org/10.1084/jem.20170997
698 15 Clapes, T. *et al.* Chemotherapy-induced transposable elements activate MDA5 to enhance
699 haematopoietic regeneration. *Nature cell biology* **23**, 704-717 (2021).
700 https://doi.org/10.1038/s41556-021-00707-9
701 16 Chiappinelli, K. B. *et al.* Inhibiting DNA Methylation Causes an Interferon Response in Cancer
702 via dsRNA Including Endogenous Retroviruses. *Cell* **162**, 974-986 (2015).
703 https://doi.org/10.1016/j.cell.2015.07.011
704 17 Roulois, D. *et al.* DNA-Demethylating Agents Target Colorectal Cancer Cells by Inducing Viral
705 Mimicry by Endogenous Transcripts. *Cell* **162**, 961-973 (2015).
706 https://doi.org/10.1016/j.cell.2015.07.056

18 Itokawa, N. *et al.* Epigenetic traits inscribed in chromatin accessibility in aged hematopoietic stem cells. *Nature communications* **13**, 2691 (2022). https://doi.org/10.1038/s41467-022-30440-2

19 Chen, Z. *et al.* Cohesin-mediated NF-kappaB signaling limits hematopoietic stem cell self-renewal in aging and inflammation. *The Journal of experimental medicine* **216**, 152-175 (2019). https://doi.org/10.1084/jem.20181505

20 Grigoryan, A. *et al.* LaminA/C regulates epigenetic and chromatin architecture changes upon aging of hematopoietic stem cells. *Genome biology* **19**, 189 (2018). https://doi.org/10.1186/s13059-018-1557-3

21 Kamminga, L. M. *et al.* The Polycomb group gene Ezh2 prevents hematopoietic stem cell exhaustion. *Blood* **107**, 2170-2179 (2006). https://doi.org/10.1182/blood-2005-09-3585

22 Adelman, E. R. *et al.* Aging Human Hematopoietic Stem Cells Manifest Profound Epigenetic Reprogramming of Enhancers That May Predispose to Leukemia. *Cancer discovery* **9**, 1080-1101 (2019). https://doi.org/10.1158/2159-8290.CD-18-1474

23 Fang, T. C. *et al.* Histone H3 lysine 9 di-methylation as an epigenetic signature of the interferon response. *The Journal of experimental medicine* **209**, 661-669 (2012). https://doi.org/10.1084/jem.20112343

24 Hansen, A. M. *et al.* H3K9 dimethylation safeguards cancer cells against activation of the interferon pathway. *Science advances* **8**, eabf8627 (2022). https://doi.org/10.1126/sciadv.abf8627

25 Avgustinova, A. *et al.* Repression of endogenous retroviruses prevents antiviral immune response and is required for mammary gland development. *Cell stem cell* **28**, 1790-1804 e1798 (2021). https://doi.org/10.1016/j.stem.2021.04.030

26 Liu, M. *et al.* Dual Inhibition of DNA and Histone Methyltransferases Increases Viral Mimicry in Ovarian Cancer Cells. *Cancer research* **78**, 5754-5766 (2018). https://doi.org/10.1158/0008-5472.CAN-17-3953

27 Schones, D. E., Chen, X., Trac, C., Setten, R. & Paddison, P. J. G9a/GLP-dependent H3K9me2 patterning alters chromatin structure at CpG islands in hematopoietic progenitors. *Epigenetics & chromatin* **7**, 23 (2014). https://doi.org/10.1186/1756-8935-7-23

28 Chou, T. C. Theoretical basis, experimental design, and computerized simulation of synergism and antagonism in drug combination studies. *Pharmacological reviews* **58**, 621-681 (2006). https://doi.org/10.1124/pr.58.3.10

29 San Jose-Eneriz, E. *et al.* Discovery of first-in-class reversible dual small molecule inhibitors against G9a and DNMTs in hematological malignancies. *Nature communications* **8**, 15424 (2017). https://doi.org/10.1038/ncomms15424

30 Higa, K. C. *et al.* Chronic interleukin-1 exposure triggers selection for Cebpa-knockout multipotent hematopoietic progenitors. *The Journal of experimental medicine* **218** (2021). https://doi.org/10.1084/jem.20200560

31 Alcazer, V. *et al.* HERVs characterize normal and leukemia stem cells and represent a source of shared epitopes for cancer immunotherapy. *American journal of hematology* **97**, 1200-1214 (2022). https://doi.org/10.1002/ajh.26647

32 Franzini, A. *et al.* The transcriptome of CMML monocytes is highly inflammatory and reflects leukemia-specific and age-related alterations. *Blood advances* **3**, 2949-2961 (2019). https://doi.org/10.1182/bloodadvances.2019000585

33 Niyongere, S. *et al.* Heterogeneous expression of cytokines accounts for clinical diversity and refines prognostication in CMML. *Leukemia* **33**, 205-216 (2019). https://doi.org/10.1038/s41375-018-0203-0

34 Pronier, E. *et al.* Macrophage migration inhibitory factor is overproduced through EGR1 in TET2(low) resting monocytes. *Communications biology* **5**, 110 (2022). https://doi.org/10.1038/s42003-022-03057-w

35 Sevin, M. *et al.* Cytokine-like protein 1-induced survival of monocytes suggests a combined strategy targeting MCL1 and MAPK in CMML. *Blood* **137**, 3390-3402 (2021). https://doi.org/10.1182/blood.2020008729

36 Mann, M. *et al.* Heterogeneous Responses of Hematopoietic Stem Cells to Inflammatory Stimuli Are Altered with Age. *Cell reports* **25**, 2992-3005 e2995 (2018). https://doi.org/10.1016/j.celrep.2018.11.056

37 Esplin, B. L. *et al.* Chronic exposure to a TLR ligand injures hematopoietic stem cells. *Journal of immunology* **186**, 5367-5375 (2011). https://doi.org/10.4049/jimmunol.1003438

38 Capone, S. *et al.* Senescent human hematopoietic progenitors show elevated expression of transposable elements and inflammatory genes. *Experimental hematology* **62**, 33-38 e36 (2018). https://doi.org/10.1016/j.exphem.2018.03.003

39 Deschamps, P. *et al.* CXCL8 secreted by immature granulocytes inhibits wildtype hematopoiesis in chronic myelomonocytic leukemia. *bioRxiv*, 2024.2003.2008.583935 (2024). https://doi.org/10.1101/2024.03.08.583935

40 Avagyan, S. *et al.* Resistance to inflammation underlies enhanced fitness in clonal hematopoiesis. *Science* **374**, 768-772 (2021). https://doi.org/10.1126/science.aba9304

41 Jakobsen, N. A. *et al.* Selective advantage of mutant stem cells in clonal hematopoiesis occurs by attenuating the deleterious effects of inflammation and aging. *bioRxiv*, 2023.2009.2012.557322 (2023). https://doi.org/10.1101/2023.09.12.557322

42 Unnikrishnan, A. *et al.* Integrative Genomics Identifies the Molecular Basis of Resistance to Azacitidine Therapy in Myelodysplastic Syndromes. *Cell reports* **20**, 572-585 (2017). https://doi.org/10.1016/j.celrep.2017.06.067

43 Ali, A. *et al.* Granulomonocytic progenitors are key target cells of azacytidine in higher risk myelodysplastic syndromes and acute myeloid leukemia. *Leukemia* **32**, 1856-1860 (2018). https://doi.org/10.1038/s41375-018-0076-2

44 Meldi, K. *et al.* Specific molecular signatures predict decitabine response in chronic myelomonocytic leukemia. *The Journal of clinical investigation* **125**, 1857-1872 (2015). https://doi.org/10.1172/JCI78752

45 Colombo, A. R. *et al.* Suppression of Transposable Elements in Leukemic Stem Cells. *Scientific reports* **7**, 7029 (2017). https://doi.org/10.1038/s41598-017-07356-9

46 Tobiasson, M. *et al.* Comprehensive mapping of the effects of azacitidine on DNA methylation, repressive/permissive histone marks and gene expression in primary cells from patients with MDS and MDS-related disease. *Oncotarget* **8**, 28812-28825 (2017). https://doi.org/10.18632/oncotarget.15807

47 Scheller, M. *et al.* Hotspot DNMT3A mutations in clonal hematopoiesis and acute myeloid leukemia sensitize cells to azacytidine via viral mimicry response. *Nat Cancer* **2**, 527-544 (2021). https://doi.org/10.1038/s43018-021-00213-9

48 Ohtani, H. *et al.* Activation of a Subset of Evolutionarily Young Transposable Elements and Innate Immunity Are Linked to Clinical Responses to 5-Azacytidine. *Cancer research* **80**, 2441-2450 (2020). https://doi.org/10.1158/0008-5472.CAN-19-1696

49 Kazachenka, A. *et al.* Epigenetic therapy of myelodysplastic syndromes connects to cellular differentiation independently of endogenous retroelement derepression. *Genome medicine* **11**, 86 (2019). https://doi.org/10.1186/s13073-019-0707-x

50 Bejar, R. *et al.* TET2 mutations predict response to hypomethylating agents in myelodysplastic syndrome patients. *Blood* **124**, 2705-2712 (2014). https://doi.org/10.1182/blood-2014-06-582809

51 Duchmann, M. *et al.* Prognostic Role of Gene Mutations in Chronic Myelomonocytic Leukemia Patients Treated With Hypomethylating Agents. *EBioMedicine* **31**, 174-181 (2018). https://doi.org/10.1016/j.ebiom.2018.04.018

52 Kelsey, M. M. G. Reconsidering LINE-1's role in cancer: does LINE-1 function as a reporter detecting early cancer-associated epigenetic signatures? *Evol Med Public Health* **9**, 78-82 (2021). https://doi.org/10.1093/emph/eoab004

53 Onishi-Seebacher, M. *et al.* Repeat to gene expression ratios in leukemic blast cells can stratify risk prediction in acute myeloid leukemia. *BMC Med Genomics* **14**, 166 (2021). https://doi.org/10.1186/s12920-021-01003-z

54 Cuellar, T. L. *et al.* Silencing of retrotransposons by SETDB1 inhibits the interferon response in acute myeloid leukemia. *The Journal of cell biology* **216**, 3535-3549 (2017). https://doi.org/10.1083/jcb.201612160

55 Gu, Z. *et al.* Silencing of LINE-1 retrotransposons is a selective dependency of myeloid leukemia. *Nature genetics* **53**, 672-682 (2021). https://doi.org/10.1038/s41588-021-00829-8

56 Esteve, P. O. *et al.* Direct interaction between DNMT1 and G9a coordinates DNA and histone methylation during replication. *Genes & development* **20**, 3089-3103 (2006). https://doi.org/10.1101/gad.1463706

57 Jiang, Q. *et al.* G9a Plays Distinct Roles in Maintaining DNA Methylation, Retrotransposon Silencing, and Chromatin Looping. *Cell reports* **33**, 108315 (2020). https://doi.org/10.1016/j.celrep.2020.108315

58 Lehnertz, B. *et al.* The methyltransferase G9a regulates HoxA9-dependent transcription in AML. *Genes & development* **28**, 317-327 (2014). https://doi.org/10.1101/gad.236794.113

59 Wingett, S. W. & Andrews, S. FastQ Screen: A tool for multi-genome mapping and quality control. *F1000Res* **7**, 1338 (2018). https://doi.org/10.12688/f1000research.15931.2

60 Ewels, P., Magnusson, M., Lundin, S. & Kaller, M. MultiQC: summarize analysis results for multiple tools and samples in a single report. *Bioinformatics* **32**, 3047-3048 (2016). https://doi.org/10.1093/bioinformatics/btw354

61 Langmead, B. & Salzberg, S. L. Fast gapped-read alignment with Bowtie 2. *Nature methods* **9**, 357-359 (2012). https://doi.org/10.1038/nmeth.1923

62 Zhang, Y. *et al.* Model-based analysis of ChIP-Seq (MACS). *Genome biology* **9**, R137 (2008). https://doi.org/10.1186/gb-2008-9-9-r137

63 Robinson, M. D., McCarthy, D. J. & Smyth, G. K. edgeR: a Bioconductor package for differential expression analysis of digital gene expression data. *Bioinformatics* **26**, 139-140 (2010). https://doi.org/10.1093/bioinformatics/btp616

64 Heinz, S. *et al.* Simple combinations of lineage-determining transcription factors prime cis-regulatory elements required for macrophage and B cell identities. *Molecular cell* **38**, 576-589 (2010). https://doi.org/10.1016/j.molcel.2010.05.004

65 Zhang, Y., Parmigiani, G. & Johnson, W. E. ComBat-seq: batch effect adjustment for RNA-seq count data. *NAR Genom Bioinform* **2**, lqaa078 (2020). https://doi.org/10.1093/nargab/lqaa078

66 Jin, Y., Tam, O. H., Paniagua, E. & Hammell, M. TEtranscripts: a package for including transposable elements in differential expression analysis of RNA-seq datasets. *Bioinformatics* **31**, 3593-3599 (2015). https://doi.org/10.1093/bioinformatics/btv422

67 Bendall, M. L. *et al.* Telescope: Characterization of the retrotranscriptome by accurate estimation of transposable element expression. *PLoS Comput Biol* **15**, e1006453 (2019). https://doi.org/10.1371/journal.pcbi.1006453

68 Anders, S., Pyl, P. T. & Huber, W. HTSeq--a Python framework to work with high-throughput sequencing data. *Bioinformatics* **31**, 166-169 (2015). https://doi.org/10.1093/bioinformatics/btu638

69 Stephens, M. False discovery rates: a new deal. *Biostatistics* **18**, 275-294 (2017). https://doi.org/10.1093/biostatistics/kxw041

855 **Figure legends**

856 **Figure 1: CMML HSPCs show a decrease in inflammatory response pathways**

857 **a)** Principal component analysis (PCA) plot of BM CD34$^+$ cells isolated from 19 CMML patients
858 at diagnosis and 12 controls, based on RNA-seq regularized log transformed expression values.
859 **b)** MA-plots showing differentially expressed genes (padj <0.1), upregulated (blue dots) or
860 downregulated (black dots) in CMML cells.
861 **c-e)** Dot plots showing selected enriched HALLMARK (total 36), GO (total 1330) and
862 senescence gene sets upregulated (positive NES, red dots) and downregulated (negative NES,
863 blue dots) in CMML cells. Gene sets are ranked by their NES and gene ration scores.
864 **f, g)** Enrichment plots for aging published gene sets. FDR, false discover rate; NES, normalized
865 enrichment score. * FDR <0.05
866

867 **Figure 2: Chromatin is remodeled in CMML HSPCs**

868 **a)** H3K9me3, **b)** H3K9me2, **c)** G9A and **d)** GLP mmunostaining in CD34$^+$ cells from CMML
869 patients and controls. Representative images and quantification of mean global
870 immunofluorescence (IF) intensity using ImageJ software are shown. Means +/- SEM from 2-
871 4 independent experiments normalized to the mean intensity of controls. Each dot represents
872 cells from a single individual, with at least 50 cells counted per sample. Bars, 3 µm. Mann-
873 Whitney test, **P<0.01; ****, P<0.0001.
874 **e)** Heat map of the differentially chromatin accessible regions in CMML patient (n=4) and
875 control (n=3) CD34$^+$ cells +/- 2.5 kb from the center of the peak (CoP).
876 **f)** Venn diagrams depicting the overlap of differentially expressed genes (DEGs) in CMML
877 HSPCs with genes assigned to gained or lost ATAC peaks (-100/+25 kb from TSS). Fisher's exact
878 test.

879 **g)** Motifs and p values for enrichment motifs of TF involed in IFN/NF-kB signaling in ATAC-seq
880 peaks unique to patients (gained) and controls (lost) using HOMER. ND: non detected
881 **h)** KEGG gene set analysis of deregulated genes that also exhibit gained (red) or loss chromatin
882 accessibility in CMML patient cells (blue).
883
884 **Figure 3: H3K9me2 is increased at TEs in CMML CD34$^+$ cells**
885 **a)** Venn diagram of peak retrieved from the calling from H3K9me2 CUT&Tag on CD34$^+$ from 4
886 patients (P) and 3 controls (CTA).
887 **b)** Repartition of the CUT&Tag peaks found exclusively in patients and controls.
888 **c)** Numbers of common peaks found exclusively in the 4 patients (red) and 3 controls (blue)
889 and numbers of TEs annotated in these peaks.
890 **d)** Enrichment or depletion of the different classes of TEs in gained or lost H3K9me2-CUT&Tag
891 peaks. The Y-axis representing the enrichment score was calculated as the log2 fold change of
892 the number of specific peaks overlapping with TEs found in patient gained or lost peaks over
893 the median number of TEs found in 1000 times the same number of randomly selected peaks
894 overlapping with TEs. Positive log2 fold change = enrichment, and negative log2 fold change =
895 depletion.
896 **e)** Repartition of the different TE classes in CUT&Tag peaks found exclusively in patients and
897 controls.
898
899 **Figure 4: the HMA and G9A/GLP inhibitor combination reduces CMML HSPC clonogenicity**
900 **a)** Treatment protocol of CD34$^+$ cells. DAC: decitabine; AZA: 5-azacytidine; UNC0638 and
901 UNC0642: G9A/GLP inhibitors; CM-272: dual DNMT1 and G9A/GLP inhibitor.

902 **b)** Dose-response effect of DAC (X-axis) and UNC0638 (color scale) on CMML CD34$^+$ colony
903 formation. Mean +/- SEM from 3 patients. Two-way ANOVA Bonferroni's multiple
904 comparisons
905 **c-d**) Chou-Talalay model of the effects of combining different doses of DAC and UNC0638. The
906 fraction affected (fa) corresponds to the proportion of colonies eliminated by the treatments.
907 The combination index (CI) is calculated by CompuSyn software (ComboSyn. Inc.) where CI<1,
908 CI=1, CI>1 indicates a synergistic, additive and antagonistic effect respectively. Mean+/- SEM
909 from 3 patients.
910 **e**) Number of colonies formed from CMML (n=28) and control (n=12) CD34$^+$ cells in the
911 absence of treatment. One dot represents a single individual. t-test
912 **f, g)** Number of colonies formed by CD34$^+$ cells from patients (f) or controls (g) after treatment
913 with 10 nM DAC and 1µM UNC0638 alone or in combination. NT: non-treated. One dot
914 represents a single individual; controls, n=12; patients, n=28. Results are normalized to the
915 number of colonies in the NT condition. Means +/- SEM. One-way ANOVA Bonferroni's
916 Multiple Comparison.
917 **h, i)** Number of colonies formed by CD34$^+$ cells from patients, n=5 (h) or controls, n=4, (i) after
918 treatment with or without (NT) 200 nM CM-272. Results are normalized to the number of
919 colonies in the NT condition. One dot represents a single individual. Means +/- SEM. t.test.
920 **p<0.01; ***p<0.001; **** p<0.0001.
921
922
923
924

925 **Figure 5: Specific targeting of CMML mutant HSCs by DAC and G9A/GLP inhibitor**
926 **combination**

927 **a)** Protocol for treatments and serial replating assays in methylcellulose using stem cell-
928 ($CD34^+CD38^-CD90^+$) or progenitor- ($CD34^+CD38^-CD90^-$)-enriched populations. P1, passage 1,
929 P2, passage 2, P3, passage 3.

930 **b)** Number of colonies formed from CMML patient stem and progenitor cells (n=3) after the
931 different passages in the presence or absence of DAC +/- UNC0638. Numbers are reported to
932 5000 cells. Mean +/- SEM. One-way ANOVA.

933 **c)** Effects of DAC and/or UNC0638 treatments on the cumulative clonogenic potential
934 ([number of colonies at P2/number of cells planted at baseline] X number cells retrieved at
935 P1) of stem and progenitor cells from patients, n=3. Mean +/- SEM. One-way ANOVA.

936 **d)** Protocol for treatments and single cell liquid culture assays using stem cell- ($CD34^+CD38^-$
937 $CD90^+$) or progenitor- ($CD34^+CD38^-CD90^-$)-enriched populations.

938 **e-g)** Single cell liquid cultures. Viability (e), proliferation index (f) and cell number distribution
939 per well at day 8 of the culture (g) of CMML patient stem cells (left panel) or progenitors (right
940 panel) treated with either DAC (green), UNC0638 (blue) or both (red), or left non-treated (NT,
941 black). n=3. Mean +/- SEM. Two-way ANOVA Bonferroni's Multiple Comparison.
942 *p<0.05; **p<0.01;***p<0.001;****p<0.0001.

943

944 **Figure 6: the drug combination selectively eliminates leukemic cells while sparing wild-type**
945 **cells in the patients.**

946 Evaluation of the variant allelic frequency of identified mutated genes with VAF >30%, after
947 14 days of culture of $CD34^+$ cells in methylcellulose (left panel) or $CD34^+CD38^-CD90^+$ stem cells
948 in liquid cultures (right panel), in the 4 conditions, as indicated. Percentage of cells with 0

949 (blue), 1 (light green and white), 2 (light and dark grey), or 3 (red) mutations. Mutation VAF
950 are indicated over each panel.
951
952 **Figure 7: Synergistic increase in TE expression in CMML patients CD34$^+$ cells after treatment**
953 **with the combination**
954 **a-e)** TE expression in RNA-seq analysis from CD34$^+$ cells from 4 patients, after treatments in
955 liquid culture with either DAC, UNC0638 or DAC+UNC0368, or left untreated (NT). **a)** Protocol
956 for treatments in liquid culture. **b)** Volcano plots showing differential TE expression
957 (pval<0.05) in the DAC+UNC0638 condition compared to NT cells. **c)** TE family (SINE, LINE, LTR,
958 DNA) repartition in differentially expressed TEs. Numbers indicate the percentage
959 represented by each family. **d)** Log2 Fold-change increase of differentially expressed TE classes
960 in the DAC+UNC0638 condition vs. NT cells. One-way ANOVA Bonferroni's Multiple
961 Comparison. **e)** Expression levels of TEs differentially expressed in the DAC+UNC0638 vs. NT
962 condition in each of the treatment conditions, sorted by TE class.
963 **f-h)** Differential analysis of ERV loci in RNA-seq data from 7 patients after treatments with
964 DAC, UNC0638 or both compared to the untreated condition (NT). **f, g)** Venn diagrams of the
965 differentially expressed ERV transcripts (pval<0.05, FC 1.5), up- (e) and down-regulated (f) in
966 each of the treated condition vs. NT, as indicated. **h)** Heat map representation of the median
967 expression level of differentially expressed HERVs in DAC+UNC0638 in the different
968 conditions. Clusters with fewer than 20 nodes were excluded from the analysis.
969 **i)** RT-qPCR analysis of mRNA expression of chosen ERV families in the different conditions. Ct
970 were normalized to HPRT, Tubulin, Gus, PPIA and/or RPL32 and reported to the NT condition.
971 One line represents a single patient. Means +/- SEM. One-way ANOVA Tukey's Multiple
972 Comparison

973 * p<0.05; **p<0.01

974

975 **Figure 8: Induction of transcriptional viral mimicry state by the combination of HMA and**
976 **G9A/GLP inhibitors.**

977 **a-e)** RNA-seq-analysis of coding genes from CD34$^+$ cells of 7 patients after 4 days of treatment
978 or not with DAC, UNC0638 or the combination. Each condition is compared to NT cells. **a)** Venn
979 diagram showing the number of common or unique DEGs in each condition. **b)** Distribution of
980 DEGs overexpressed (red) and downregulated (blue). **c, d)** GSE analysis of pathways enriched
981 in upregulated (c) and downregulated (d) genes in DAC+UNC0638 vs. NT. **e)** Enrichment
982 analysis of different IFN/antiviral signatures by single sample gene-set variation analysis
983 (ssGSVA). **f)** mRNA expression level of IFNB1, IRF9 and IRF9 measured by RT-qPCR. Ct were
984 normalized by custom housekeeping genes (HPRT, Tubulin, Gus, PPIA and/or RPL32) and
985 reported to the NT condition. Each line represents a single patient. Means +/- SEM. One-way
986 ANOVA Dunnett's multiple comparison* p<0.05

987

988 **Figure 9: IFN signaling is activated by the HMA and G9A/GLP inhibitor combination.**

989 Representative images and quantification of the mean overall immunofluorescence (IF)
990 intensity of **a)** IRF3, **b)** IRF7, **c)** STAT1, **d)** pSTAT1 and **e)** dsRNAs in patient CD34$^+$ cells after 4
991 days of culture. Results are reported to the mean IF intensity in the NT condition. N= 2
992 patients. Bars, 3 µm. Quantifications were performed using ImageJ software. Violin plots
993 representing the mean IF intensity of each cell. At least 45 cells counted per sample. Dotted
994 lines: median and 25th and 75th percentiles. One-way ANOVA Bonferroni's Multiple
995 Comparison. **p<0.01;****p<0.0001.

996

997 **Figure 10: IFN signaling is required for HMA and G9A/GLP inhibitor combination-induced cell**
998 **death.**

999 **a)** Protocol scheme for the treatments with DAC +/- UNC0638 and blocking IFN receptor
1000 (IFNAR2) antibodies. The anti-IFNAR2 antibody (1µg/ml) was added on days 2 and 4 and the
1001 cells were seeded in methylcellulose on day 4.

1002 **b)** Number of colonies at passages 1 and 2, reported to the non-treated condition.

1003 **c)** Cumulative potential at passage 2. Results are reported to those obtained in the NT
1004 condition. Mean +/- SEM ; n=6 patients. One-way
1005 ANOVA Bonferroni's multiple Comparison. $p<0.05$; $^{**}p<0.01$;$^{****}p<0.0001$.

1006 **d)** Model illustrating the increase in H3K9me2 at TEs and repression of immune-associated
1007 transcripts in CMML HSPCs compared with age-matched healthy HSPCs (left). The mechanism
1008 repressing inflammatory gene is unknown but independent of H3K9me2. TEs are repressed by
1009 both H3K9me2 and DNA methylation in CMML cells, as shown by their reexpression only upon
1010 treatment with a combination of HMA and G9A/GLP inhibitors. Reexpression of TEs results in
1011 dsRNA formation, induction of IFN signaling and reactivation of the innate immune response
1012 in CMML HSCs, selectively targeting mutated cells while preserving residual wild-type HSCs.
1013 Dark blue cell: healthy donor HSPC. Red cells: CMML HSPC. Red cell with a yellow star: CMML
1014 mutated HSC. These cells enter in apoptosis upon treatment with the combination. Light blue
1015 cell: non-mutated HSC in CMML patients. Dark blue cell: healthy donor cell.

Figure 1

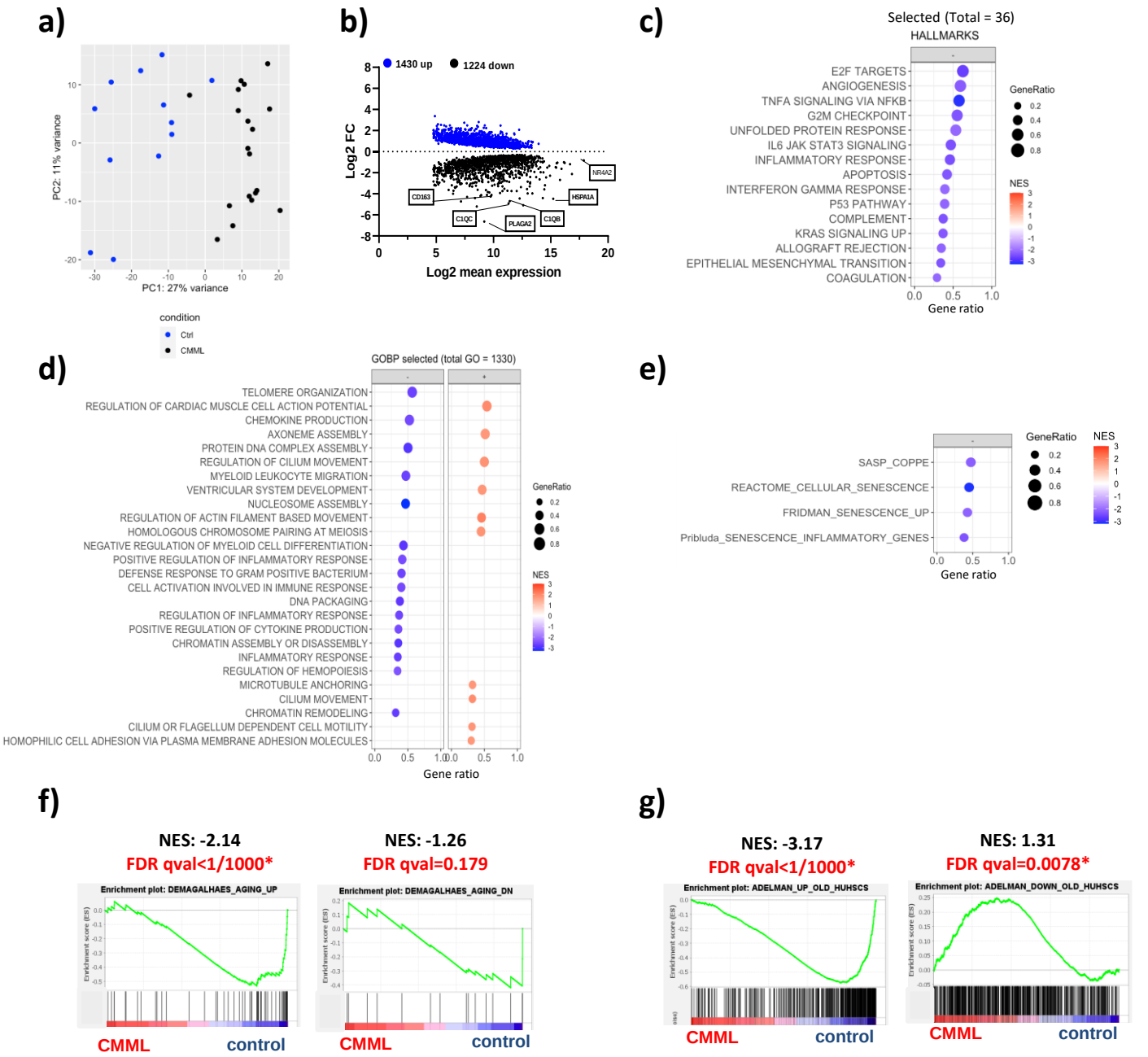
a)
PC2: 11% variance
PC1: 27% variance
condition
Ctrl
CMML
b)
1430 up
1224 down
Log2 FC
Log2 mean expression
NR4A2
CD163
HSPA1A
C1QC
PLAGA2
C1QB
c)
Selected (Total = 36)
HALLMARKS
E2F TARGETS
ANGIOGENESIS
TNFA SIGNALING VIA NFKB
G2M CHECKPOINT
UNFOLDED PROTEIN RESPONSE
IL6 JAK STAT3 SIGNALING
INFLAMMATORY RESPONSE
APOPTOSIS
INTERFERON GAMMA RESPONSE
P53 PATHWAY
COMPLEMENT
KRAS SIGNALING UP
ALLOGRAFT REJECTION
EPITHELIAL MESENCHYMAL TRANSITION
COAGULATION
Gene ratio
GeneRatio
NES
d)
GOBP selected (total GO = 1330)
TELOMERE ORGANIZATION
REGULATION OF CARDIAC MUSCLE CELL ACTION POTENTIAL
CHEMOKINE PRODUCTION
AXONEME ASSEMBLY
PROTEIN DNA COMPLEX ASSEMBLY
REGULATION OF CILIUM MOVEMENT
MYELOID LEUKOCYTE MIGRATION
VENTRICULAR SYSTEM DEVELOPMENT
NUCLEOSOME ASSEMBLY
REGULATION OF ACTIN FILAMENT BASED MOVEMENT
HOMOLOGOUS CHROMOSOME PAIRING AT MEIOSIS
NEGATIVE REGULATION OF MYELOID CELL DIFFERENTIATION
POSITIVE REGULATION OF INFLAMMATORY RESPONSE
DEFENSE RESPONSE TO GRAM POSITIVE BACTERIUM
CELL ACTIVATION INVOLVED IN IMMUNE RESPONSE
DNA PACKAGING
REGULATION OF INFLAMMATORY RESPONSE
POSITIVE REGULATION OF CYTOKINE PRODUCTION
CHROMATIN ASSEMBLY OR DISASSEMBLY
INFLAMMATORY RESPONSE
REGULATION OF HEMOPOIESIS
MICROTUBULE ANCHORING
CILIUM MOVEMENT
CHROMATIN REMODELING
CILIUM OR FLAGELLUM DEPENDENT CELL MOTILITY
HOMOPHILIC CELL ADHESION VIA PLASMA MEMBRANE ADHESION MOLECULES
Gene ratio
GeneRatio
NES
e)
SASP_COPPE
REACTOME_CELLULAR_SENESCENCE
FRIDMAN_SENESCENCE_UP
Pribluda_SENESCENCE_INFLAMMATORY_GENES
Gene ratio
GeneRatio
NES
f)
NES: -2.14
FDR qval<1/1000*
Enrichment plot: DEMAGALHAES_AGING_UP
CMML
control
NES: -1.26
FDR qval=0.179
Enrichment plot: DEMAGALHAES_AGING_DN
CMML
control
g)
NES: -3.17
FDR qval<1/1000*
Enrichment plot: ADELMAN_UP_OLD_HUHSCS
CMML
control
NES: 1.31
FDR qval=0.0078*
Enrichment plot: ADELMAN_DOWN_OLD_HUHSCS
CMML
control

Figure 2

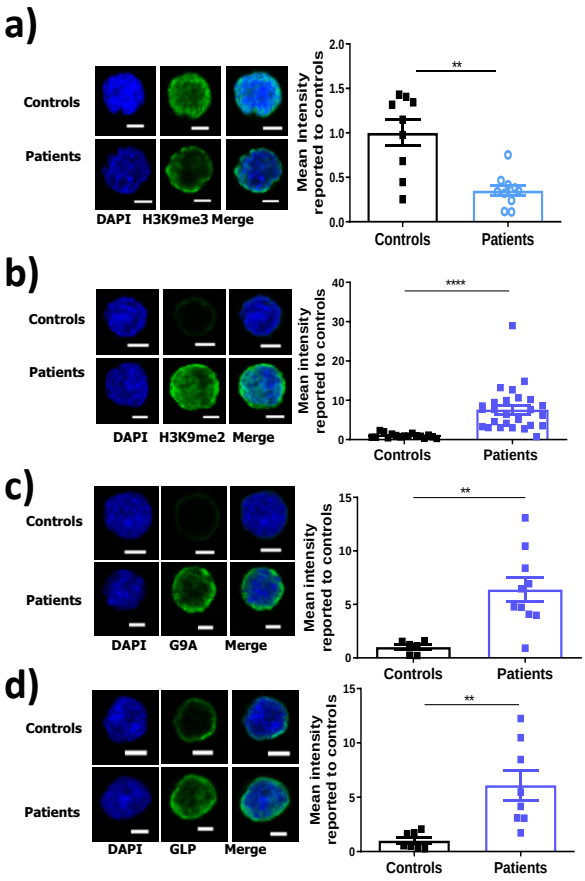

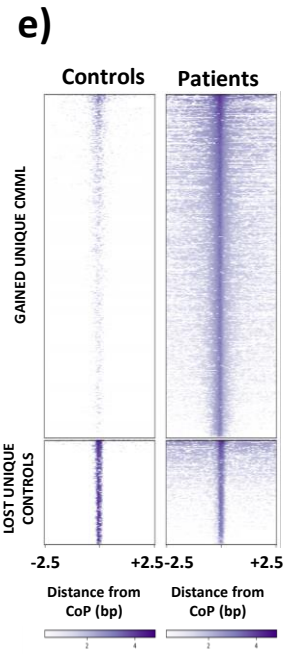

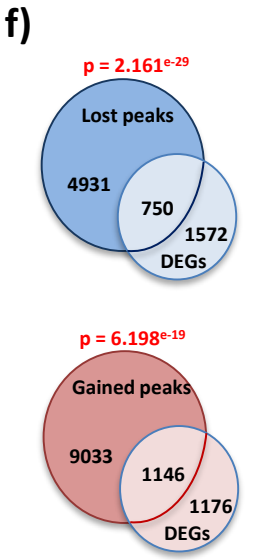

g)

Motif	Transcription factor	Lost	Gained
GGGAAGTGAAAC	PU1-IRF	1^{e-53}	1^{e-5}
AGTTTCAGTTTC	IRF3	1^{e-27}	1^{e-5}
GAAAGTGAAAGT	IRF1	1^{e-25}	1^{e-7}
GGAAATTCCC	NFkB-p65-Rel	1^{e-11}	ND
AGGGGATTTCCC	NFkB-p65	1^{e-11}	ND
AGTTTCAGTTTC	ISRE	1^{e-10}	1^{e-4}
GGGGGAATCCCC	NFkB-p50,p52	1^{e-4}	ND

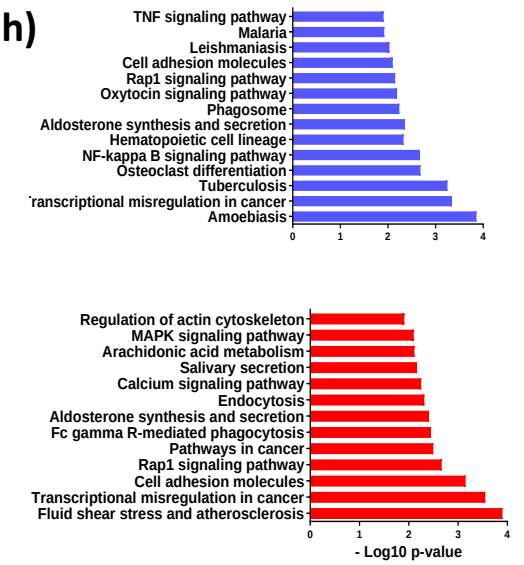

Figure 3

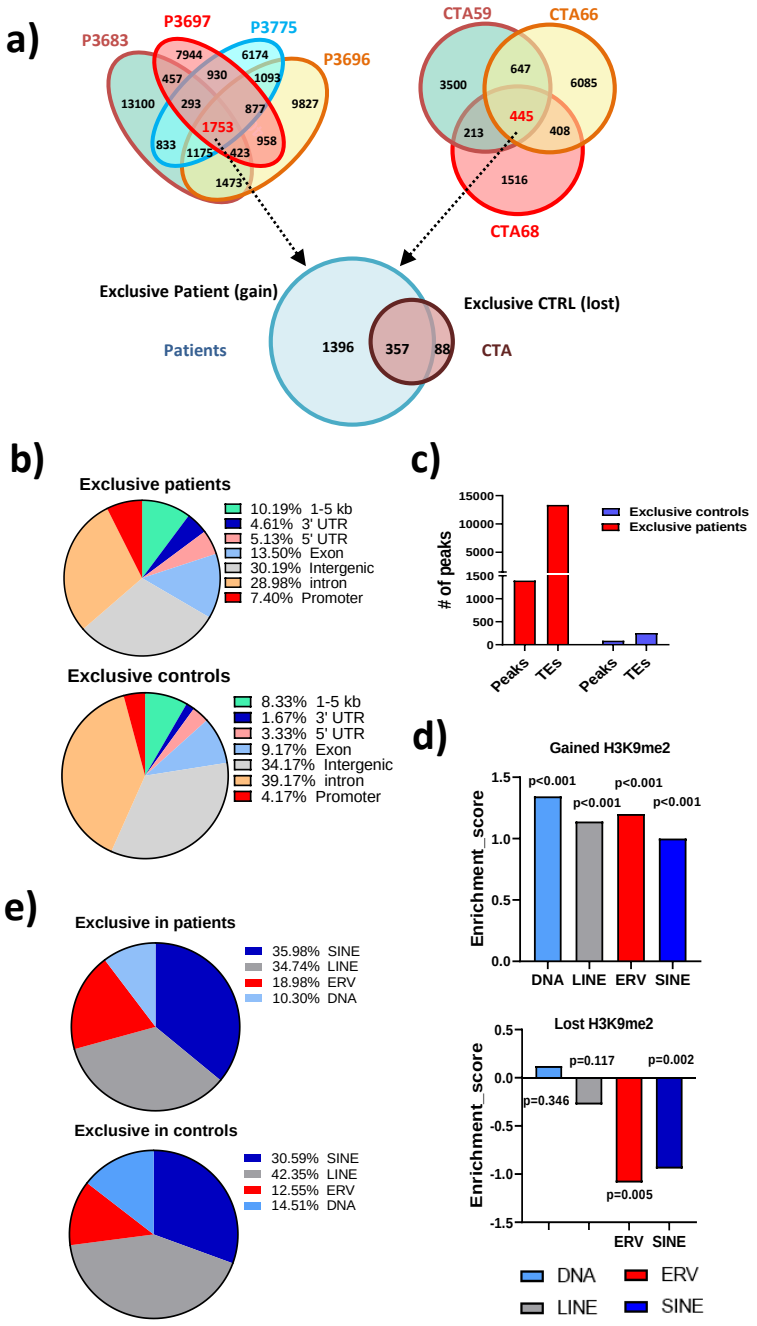
a)
P3683
P3697
P3775
P3696
7944
6174
457
930
1093
13100
293
877
9827
1753
833
1175
423
958
1473
CTA59
CTA66
CTA68
3500
647
6085
445
213
408
1516
Exclusive Patient (gain)
Exclusive CTRL (lost)
Patients
1396
357
88
CTA
b)
Exclusive patients
10.19% 1-5 kb
4.61% 3' UTR
5.13% 5' UTR
13.50% Exon
30.19% Intergenic
28.98% intron
7.40% Promoter
Exclusive controls
8.33% 1-5 kb
1.67% 3' UTR
3.33% 5' UTR
9.17% Exon
34.17% Intergenic
39.17% intron
4.17% Promoter
c)
# of peaks
Exclusive controls
Exclusive patients
Peaks
TEs
Peaks
TEs
d)
Gained H3K9me2
Enrichment_score
p<0.001
p<0.001
p<0.001
p<0.001
DNA
LINE
ERV
SINE
Lost H3K9me2
Enrichment_score
p=0.117
p=0.002
p=0.346
p=0.005
ERV
SINE
DNA
ERV
LINE
SINE
e)
Exclusive in patients
35.98% SINE
34.74% LINE
18.98% ERV
10.30% DNA
Exclusive in controls
30.59% SINE
42.35% LINE
12.55% ERV
14.51% DNA

Figure 4

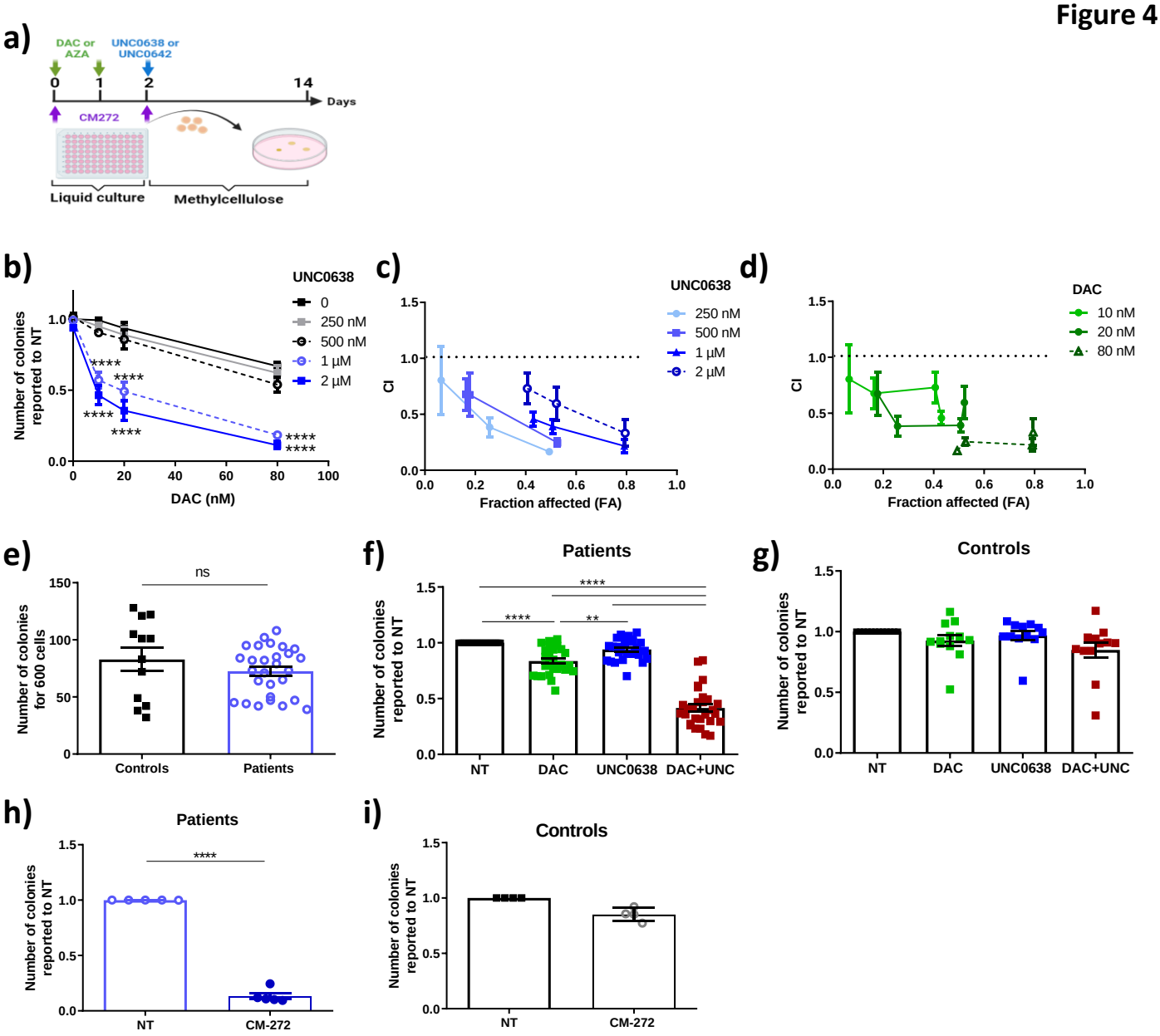
a)
DAC or AZA
UNC0638 or UNC0642
0
1
2
14
Days
CM272
Liquid culture
Methylcellulose
b)
UNC0638
0
250 nM
500 nM
1 µM
2 µM
Number of colonies reported to NT
DAC (nM)
c)
UNC0638
250 nM
500 nM
1 µM
2 µM
CI
Fraction affected (FA)
d)
DAC
10 nM
20 nM
80 nM
CI
Fraction affected (FA)
e)
ns
Number of colonies for 600 cells
Controls
Patients
f)
Patients
Number of colonies reported to NT
NT
DAC
UNC0638
DAC+UNC
g)
Controls
Number of colonies reported to NT
NT
DAC
UNC0638
DAC+UNC
h)
Patients
Number of colonies reported to NT
NT
CM-272
i)
Controls
Number of colonies reported to NT
NT
CM-272

Figure 5

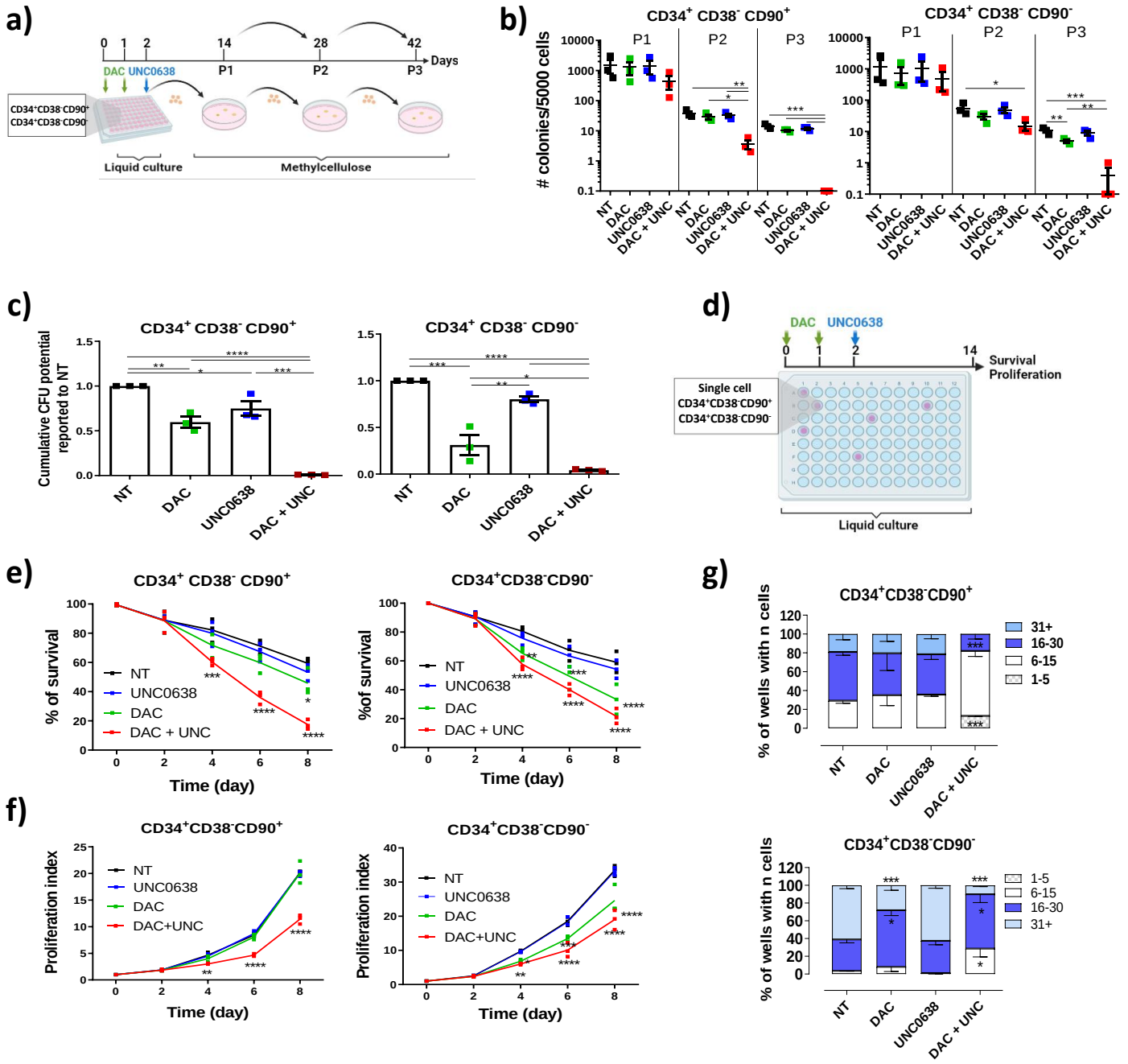
a)
0 1 2 14 28 42
Days
DAC UNC0638
P1 P2 P3
CD34+CD38-CD90+
CD34+CD38-CD90-
Liquid culture
Methylcellulose
b)
CD34+ CD38- CD90+
CD34+ CD38- CD90-
P1 P2 P3
colonies/5000 cells
NT DAC UNC0638 DAC + UNC
c)
CD34+ CD38- CD90+
CD34+ CD38- CD90-
Cumulative CFU potential reported to NT
NT DAC UNC0638 DAC + UNC
d)
DAC UNC0638
0 1 2 14
Survival Proliferation
Single cell
CD34+CD38-CD90+
CD34+CD38-CD90-
Liquid culture
e)
CD34+ CD38- CD90+
CD34+CD38-CD90-
% of survival
%of survival
NT
UNC0638
DAC
DAC + UNC
Time (day)
f)
CD34+CD38-CD90+
CD34+CD38-CD90-
Proliferation index
NT
UNC0638
DAC
DAC+UNC
Time (day)
g)
CD34+CD38-CD90+
CD34+CD38-CD90-
% of wells with n cells
31+
16-30
6-15
1-5
NT DAC UNC0638 DAC + UNC

Figure 6

CD34⁺ methylcellulose colonies

Patient #3440
TET2-K1338X (54%) RUNX1-S114L (61%) SRSF295H (17%)

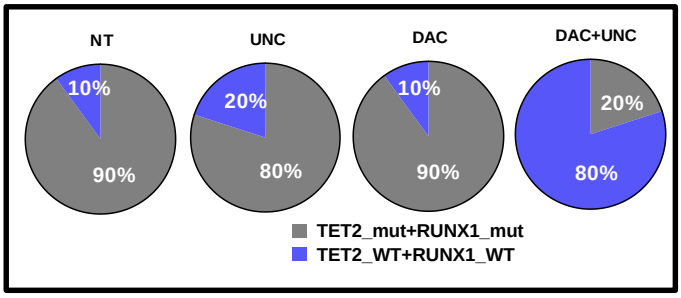

Patient #3562
KRAS-G12D (30%) TET2-S407fs (9%) RUNX1-Y285F (11%)

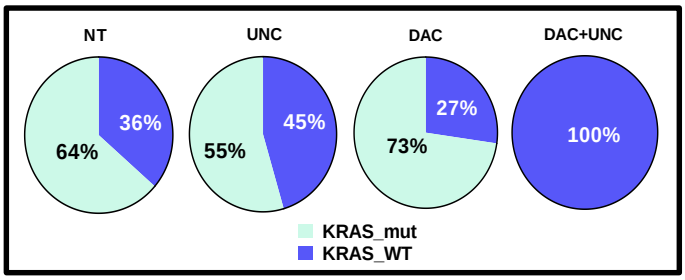

Patient #3564
TET2-L1229P (41%) SRSF2-P95R (37%)

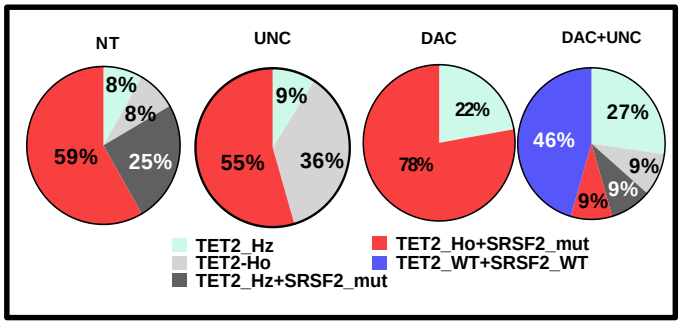

CD34⁺C38⁻CD90⁺ single cell liquid cultures

Patient #3459
TET2-H1480Q Hz (44%) ASXL1(2%)

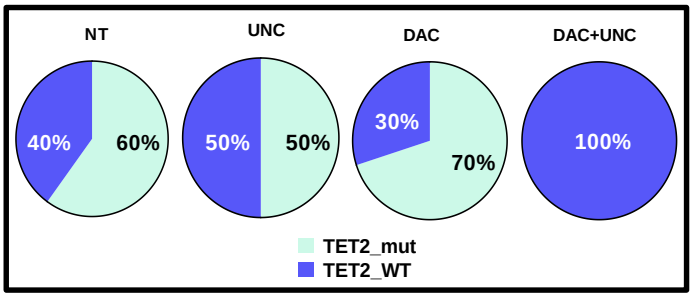

Patient #3480
DNMT3A-DEL-G (34%) TET2-H1380R (37%)

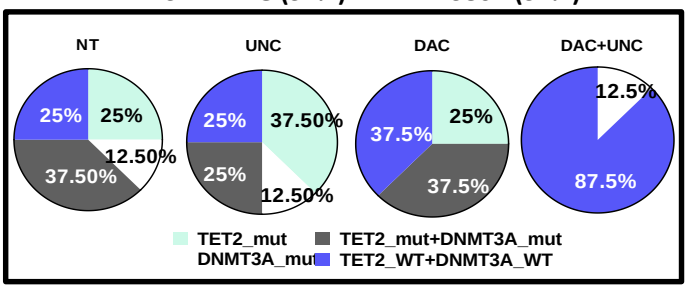

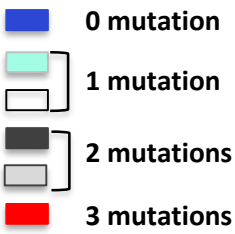

Figure 7

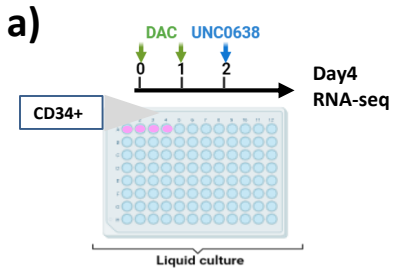
a)
DAC
UNC0638
0
1
2
Day4
RNA-seq
CD34+
Liquid culture

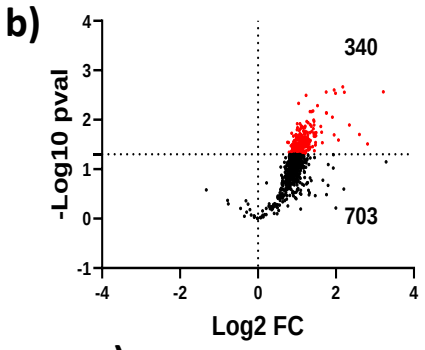
b)
340
703
-Log10 pval
Log2 FC

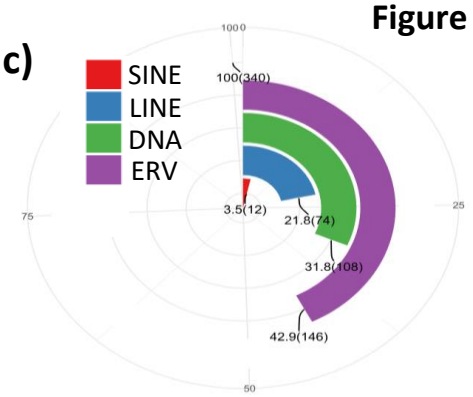
c)
SINE
LINE
DNA
ERV
100(340)
3.5(12)
21.8(74)
31.8(108)
42.9(146)

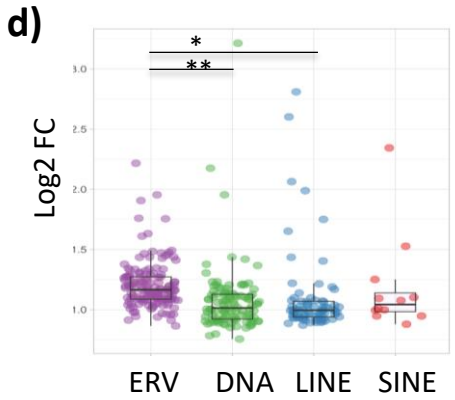
d)
Log2 FC
ERV
DNA
LINE
SINE

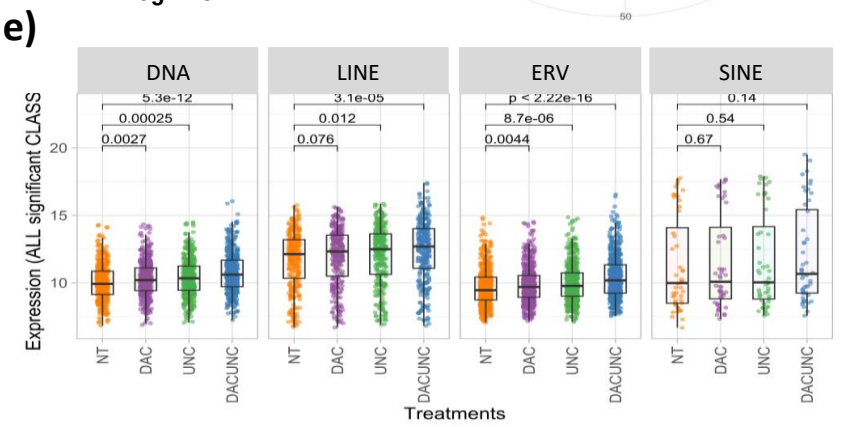
e)
DNA
LINE
ERV
SINE
Expression (ALL significant CLASS
Treatments
NT
DAC
UNC
DACUNC

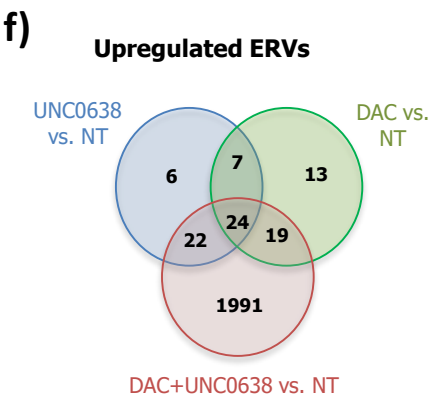
f)
Upregulated ERVs
UNC0638 vs. NT
DAC vs. NT
DAC+UNC0638 vs. NT
6
7
13
24
22
19
1991

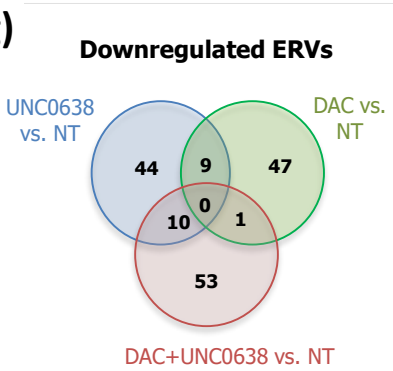
g)
Downregulated ERVs
UNC0638 vs. NT
DAC vs. NT
DAC+UNC0638 vs. NT
44
9
47
0
10
1
53

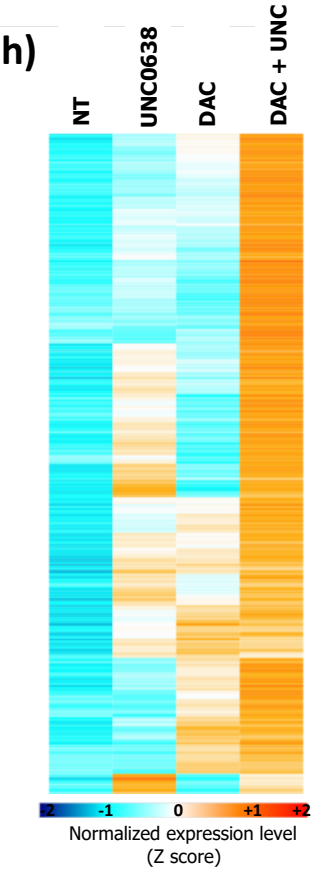
h)
NT
UNC0638
DAC
DAC + UNC
Normalized expression level
(Z score)

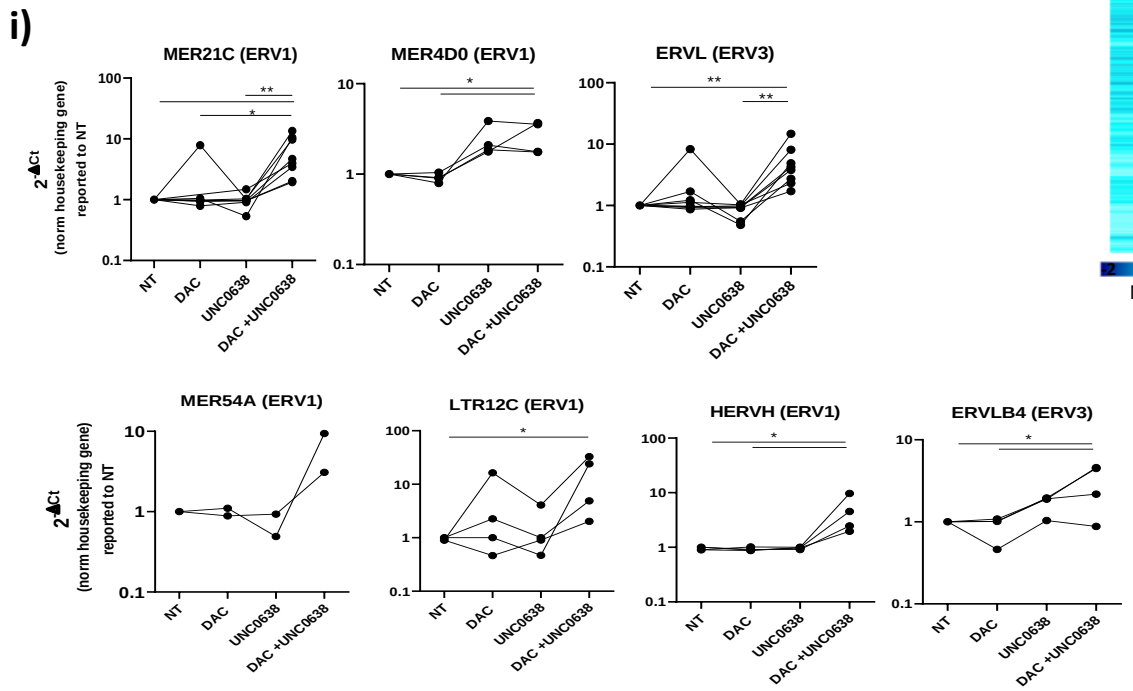
i)
MER21C (ERV1)
MER4D0 (ERV1)
ERVL (ERV3)
MER54A (ERV1)
LTR12C (ERV1)
HERVH (ERV1)
ERVLB4 (ERV3)
2-ΔCt
(norm housekeeping gene)
reported to NT
NT
DAC
UNC0638
DAC +UNC0638

Figure 8

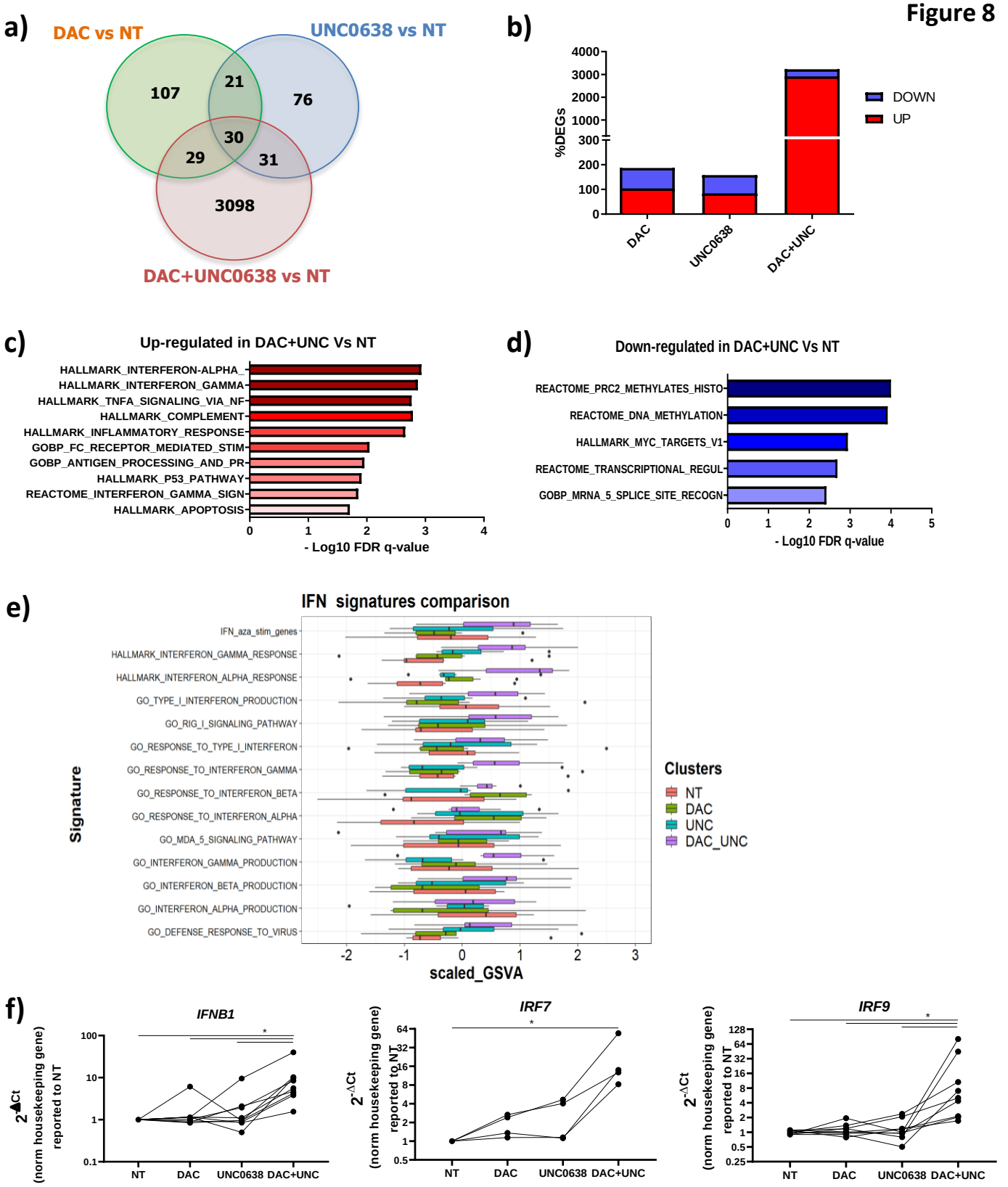
a)
DAC vs NT
UNC0638 vs NT
DAC+UNC0638 vs NT
107
21
76
30
29
31
3098
b)
%DEGs
DOWN
UP
DAC
UNC0638
DAC+UNC
c)
Up-regulated in DAC+UNC Vs NT
HALLMARK_INTERFERON-ALPHA_
HALLMARK_INTERFERON_GAMMA
HALLMARK_TNFA_SIGNALING_VIA_NF
HALLMARK_COMPLEMENT
HALLMARK_INFLAMMATORY_RESPONSE
GOBP_FC_RECEPTOR_MEDIATED_STIM
GOBP_ANTIGEN_PROCESSING_AND_PR
HALLMARK_P53_PATHWAY
REACTOME_INTERFERON_GAMMA_SIGN
HALLMARK_APOPTOSIS
- Log10 FDR q-value
d)
Down-regulated in DAC+UNC Vs NT
REACTOME_PRC2_METHYLATES_HISTO
REACTOME_DNA_METHYLATION
HALLMARK_MYC_TARGETS_V1
REACTOME_TRANSCRIPTIONAL_REGUL
GOBP_MRNA_5_SPLICE_SITE_RECOGN
- Log10 FDR q-value
e)
IFN signatures comparison
IFN_aza_stim_genes
HALLMARK_INTERFERON_GAMMA_RESPONSE
HALLMARK_INTERFERON_ALPHA_RESPONSE
GO_TYPE_I_INTERFERON_PRODUCTION
GO_RIG_I_SIGNALING_PATHWAY
GO_RESPONSE_TO_TYPE_I_INTERFERON
GO_RESPONSE_TO_INTERFERON_GAMMA
GO_RESPONSE_TO_INTERFERON_BETA
GO_RESPONSE_TO_INTERFERON_ALPHA
GO_MDA_5_SIGNALING_PATHWAY
GO_INTERFERON_GAMMA_PRODUCTION
GO_INTERFERON_BETA_PRODUCTION
GO_INTERFERON_ALPHA_PRODUCTION
GO_DEFENSE_RESPONSE_TO_VIRUS
Signature
scaled_GSVA
Clusters
NT
DAC
UNC
DAC_UNC
f)
IFNB1
IRF7
IRF9
2-ΔCt (norm housekeeping gene) reported to NT
NT
DAC
UNC0638
DAC+UNC

Figure 9

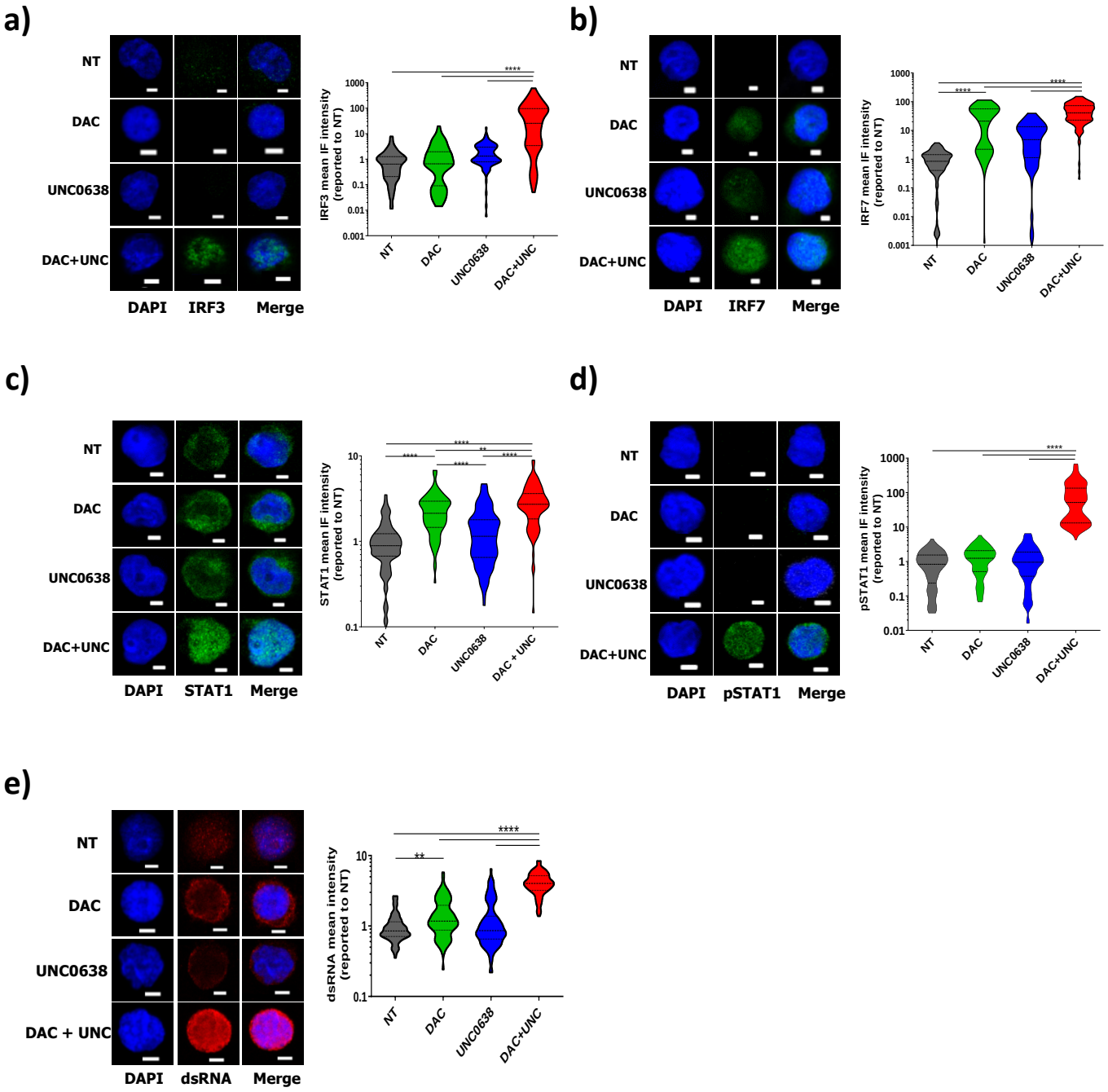
a)
NT
DAC
UNC0638
DAC+UNC
DAPI
IRF3
Merge
IRF3 mean IF intensity (reported to NT)
1000
100
10
1
0.1
0.01
0.001
****
NT
DAC
UNC0638
DAC+UNC
b)
NT
DAC
UNC0638
DAC+UNC
DAPI
IRF7
Merge
IRF7 mean IF intensity (reported to NT)
1000
100
10
1
0.1
0.01
0.001
****
****
NT
DAC
UNC0638
DAC+UNC
c)
NT
DAC
UNC0638
DAC+UNC
DAPI
STAT1
Merge
STAT1 mean IF intensity (reported to NT)
10
1
0.1
****
**
****
****
****
NT
DAC
UNC0638
DAC + UNC
d)
NT
DAC
UNC0638
DAC+UNC
DAPI
pSTAT1
Merge
pSTAT1 mean IF intensity (reported to NT)
1000
100
10
1
0.1
0.01
****
NT
DAC
UNC0638
DAC+UNC
e)
NT
DAC
UNC0638
DAC + UNC
DAPI
dsRNA
Merge
dsRNA mean intensity (reported to NT)
10
1
0.1
**
****
NT
DAC
UNC0638
DAC+UNC

Figure 10

a)

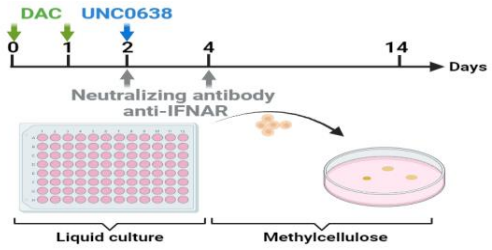

c)

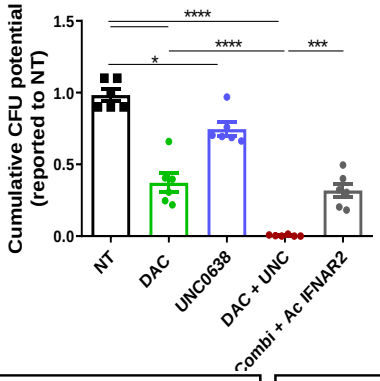

b)

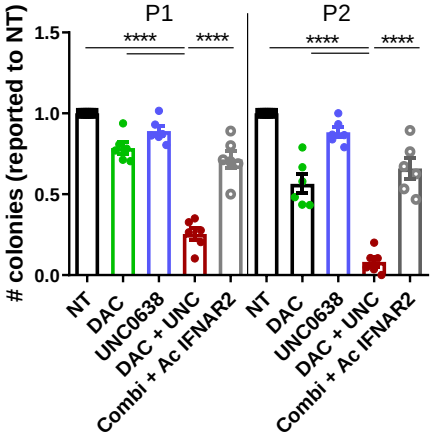
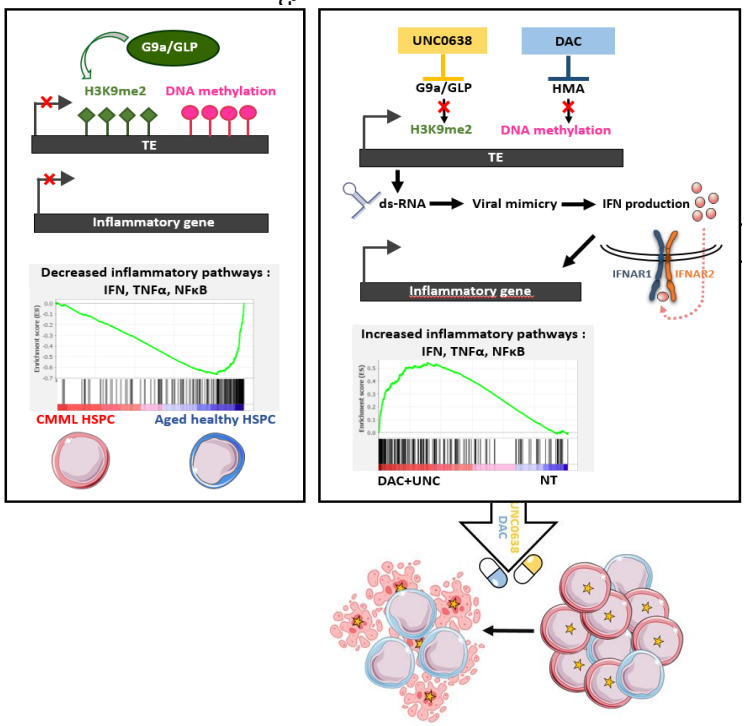
d)